

***MYTHO*: An Uncharacterized FoxO-Dependent Gene that Controls
Autophagy and Skeletal Muscle Mass**

Felipe Eduardo Broering

Division of Experimental Medicine
McGill University, Montreal
Quebec, Canada
August 2021

A thesis submitted to McGill University in partial fulfilment of the requirements of the
degree of Master of Science

© Felipe Eduardo Broering, 2021

TABLE OF CONTENTS

ABSTRACT	4
RÉSUMÉ	6
ACKNOWLEDGEMENTS	8
LIST OF ABBREVIATIONS	10
CONTRIBUTION OF AUTHORS	13
SECTION 1: INTRODUCTION AND LITERATURE REVIEW	15
1.1. Introduction	15
1.2. Skeletal muscle: structure and classification	18
1.3. Regulation of skeletal muscle mass	20
<i>1.3.1. Protein synthesis</i>	<i>20</i>
<i>1.3.2. Protein degradation</i>	<i>21</i>
1.4. Ubiquitin-proteasome pathway	23
1.5. Autophagy-lysosome pathway	25
1.6. Autophagy and skeletal muscle function	29
1.7. FoxO transcription factors and MYTHO	31
1.8. Aims of this study	34
SECTION 2: MATERIALS AND METHODS	35
2.1. Animal procedures and AAV injection in skeletal muscle	35
2.2. Tissue collection	35
2.3. Immunoblotting	36
2.4. RNA extraction and quantitative real-time PCR	37
2.5. Muscle sections for histology analysis	37

2.6.	<i>In situ</i> determination of fibre typology	38
2.7.	Transmission electron microscopy	38
2.8.	<i>In situ</i> assessment of muscle contractile function.....	39
2.9.	Statistical analyses	40
SECTION 3: RESULTS		41
3.1.	Verification of MYTHO knockdown in limb muscles	41
3.2.	Effects of MYTHO knockdown on muscle mass, muscle histology and fibre size	41
3.3.	Effects of MYTHO knockdown on muscle fibre type.....	42
3.4.	Effects of MYTHO knockdown on markers of muscle fibre regeneration	43
3.5.	Effects of MYTHO knockdown on muscle ultrastructure.....	43
3.6.	Effects of MYTHO knockdown on the autophagy pathway.....	43
3.7.	Effects of MYTHO knockdown on muscle contractility	44
SECTION 4: DISCUSSION.....		45
SECTION 5: REFERENCES		54
SECTION 6: TABLES		66
SECTION 7: FIGURES		68
SECTION 8: FIGURE LEGENDS		90

ABSTRACT

Skeletal muscles make up a large proportion of total body mass and act as very important reserves of energy substrates that are needed to support critical organ function. Muscle mass is determined by the balance between protein synthesis and protein degradation; enhanced degradation under catabolic conditions leads to loss of muscle mass, or atrophy. Protein degradation inside muscle fibres is regulated by the ubiquitin-proteasome, calpains, caspases, and autophagy-lysosome proteolytic pathways. Autophagy is the mechanism that removes cytoplasmic proteins and damaged cellular organelles. Autophagy is generally thought of as a pro-survival process, although excessive activation can result in severe losses in muscle mass. Recycling of proteins and organelles by autophagy is accomplished through the formation of double membrane vesicles called autophagosomes that surround damaged components and deliver them to lysosomes for degradation and recycling. Autophagy is regulated at the transcriptional levels mainly by forkhead box protein O (FoxO) transcription factors and at post-transcriptional level by the protein kinase B (AKT) and mammalian target of rapamycin (mTOR) pathways.

To identify novel FoxO-dependent genes that regulate autophagy in skeletal muscles, we performed pilot experiments on atrophic models in mice which revealed the presence of an uncharacterized gene whose expression is significantly upregulated in FoxO-dependent manner in atrophic muscles. This gene is known as *D230025D16Rik* in mice and *C16orf70* in humans. Experiments by our collaborators on *C. elegans* revealed that this gene promotes autophagy and survival, hence named MYTHO (Macroautophagy regulator and YouTH Optimizer). They showed that MYTHO expression is significantly elevated in skeletal muscles of mice undergoing acute starvation (24 hours). Moreover, using bioinformatic tools, we found that MYTHO expression in skeletal muscles is significantly increased in mice in catabolic conditions such as cancer cachexia. This thesis addresses the expression and functional

importance of MYTHO in the regulation of skeletal muscle mass, function, and autophagosome formation under basal conditions.

To study the functional importance of MYTHO in skeletal muscle mass and function, we used a loss-of-function approach in which adeno-associated viruses (AAVs) expressing short hairpin RNA targeting murine MYTHO (shRNA-MYTHO) were injected into limb muscles of wild type C57BL/6J adult male mice. Knockdown of MYTHO expression in skeletal muscles for three months was associated with an increase in muscle mass but significant decrease in muscle contractility. Histological examination of muscle sections showed significant increase in the number of relatively small size fibres which contained one or more central nuclei and the presence of few necrotic fibres infiltrated by inflammatory cells. MYTHO knockdown was also associated with a decrease in the levels of type IIA myosin heavy chain (MyHC) isoform and increased neonatal MyHC isoform expression. Transmission electron microscopy (TEM) examination of muscles with MYTHO knockdown revealed significant accumulation of tubular aggregates structures and abnormally shaped intermyofibrillar mitochondria. These results suggest that MYTHO plays an important role in the regulation of skeletal muscle fibre integrity as well as sarcoplasmic reticulum. Our results also indicate that MYTHO is an essential regulator of skeletal muscle homeostasis through yet to be determined mechanisms.

RÉSUMÉ

Les muscles squelettiques représentent une grande proportion de la masse corporelle totale et agissent comme des réserves très importantes des substrats énergétiques nécessaires pour soutenir les fonctions essentielles de multiples organes. La masse musculaire est déterminée par l'équilibre entre la synthèse des protéines et la dégradation des protéines ; une augmentation de la dégradation des protéines lors de conditions cataboliques conduit à une perte de masse musculaire, ou atrophie. La dégradation des protéines à l'intérieur des fibres musculaires est régulée par le système ubiquitine-protéasome, les calpaïnes, les caspases et la voie lysosome-autophagie. L'autophagie est le mécanisme responsable de l'élimination des protéines cytoplasmiques et des organites cellulaires endommagés. L'autophagie est un processus nécessaire à la survie, bien qu'une activation excessive puisse entraîner d'importantes pertes de masse musculaire. L'autophagie est régulée au niveau transcriptionnel par les facteurs de transcription forkhead box protéine (FoxO) et au niveau post-transcriptionnel par les voies régulées par la protéine kinase B (AKT) et la cible chez les mammifères de la rapamycine (mTOR).

Pour identifier de nouveaux gènes sous le contrôle de FoxO qui régulent l'autophagie dans les muscles squelettiques, nous avons réalisé des expériences pilotes sur de modèles d'atrophie chez la souris qui ont révélé la présence d'un gène non caractérisé dont l'expression est significativement augmentée de manière dépendante de FoxO dans les muscles atrophiés. Ce gène est connu sous le nom de D230025C16Rik chez la souris et C16orf70 chez l'humain. Les expériences de nos collaborateurs sur *C. elegans* ont révélé que ce gène régule positivement l'autophagie et la survie, d'où le nom de MYTHO (*Macroautophagy regulator and YouTH Optimizer*). Ils ont également montré que l'expression de MYTHO est significativement augmentée dans les muscles squelettiques des souris exposées à une jeûne de 24 heures. De plus, à l'aide d'outils bio-informatiques, nous avons constaté que l'expression de MYTHO

musculaire est augmentée de manière significative chez les souris atteintes de cachexie causée par le cancer. Cette thèse s'intéresse à la caractérisation de l'expression et de l'importance fonctionnelle de MYTHO dans la régulation de la masse musculaire squelettique, de la fonction et de la formation d'autophagosomes dans des conditions basales.

Pour étudier l'importance fonctionnelle de MYTHO dans la régulation de la masse et la fonction *in vivo* des muscles squelettiques, nous avons utilisé une approche de perte de fonction dans laquelle des virus adéno-associés (VAA) exprimant un ARN court en épingle à cheveux ciblant MYTHO ont été injectés dans les muscles des membres de souris mâles adultes de type sauvage C57BL/6J. La réduction de l'expression de MYTHO pendant trois mois a causé une augmentation de la masse musculaire et une diminution significative de la contractilité musculaire. L'examen histologique de coupes musculaires a révélé une augmentation significative du nombre de fibres relativement petites de taille présentant un ou plusieurs noyaux centraux et la présence de quelques fibres nécrotiques infiltrées par des cellules inflammatoires. La déplétion de MYTHO a également induit une diminution de l'expression des chaînes lourdes de myosine de type IIa et une augmentation de l'expression des chaînes lourdes de myosine néonatales. L'examen en microscopie électronique des muscles déplétés en MYTHO a révélé une accumulation significative des structures d'agrégats tubulaires et des mitochondries inter-myofibrillaires anormales. Ces résultats suggèrent que MYTHO joue un rôle important dans la régulation de l'intégrité des fibres musculaires squelettiques, incluant celle du réticulum sarcoplasmique. Nos résultats indiquent également que MYTHO est un régulateur positif de la contractilité des muscles squelettiques par des mécanismes qui restent encore à déterminer.

ACKNOWLEDGEMENTS

At the end of the day, it's never a one-person work and there are so many people to thank. I would like to start mentioning two persons who, among many other qualities, share an enormous sense of generosity and were crucial throughout my training in research: my supervisor, Dr. Sabah N. A. Hussain, and my teammate, Dr. Jean-Philippe Leduc-Gaudet.

Professor Hussain has a big heart. Between football matches and laughs, and lots and lots of hard work, one can see a resilient and sensitive soul, always ready to help others. An extraordinary scientist that not only McGill but any other world-class university would be proud to have as faculty member. I thank him for his support over the past few years, for the words of wisdom, and for the great opportunities he has gifted me, but most of all I am thankful for the opportunity of being part of "Sabah's team".

Jean-Philippe, for his turn, started by giving me gloves and *tuque*, two essentials for the first winter a Brazilian would face in Canada. He also was kind enough to train a not-so-young guy to perform lab experiments and I thank him for all his support. Among the many things, I can cite a few such as histology and western blot techniques and operating a transmission electron microscope. Just as Sabah, he is one of the most dedicated and talented professionals who I ever met.

I would like also to thank Dominique Mayaki, a "wise wizard" who runs Dr. Hussain's lab, and who was always there for me and for everyone else. One can be amazed by his knowledge and multitasking skills, designing primers, cultivating cells, managing the busy biobar, holding down the fort. On the other side of the bench, the experienced Laurent Huck had a lot to teach us likewise, and I am grateful for his contributions to my work. My undergrad teammates, Tomer Jordi Chaffer and Marwa El Sheikh, are the evidence of talent in young generations. I thank them for their great support and for the pleasant company. It is easy to foresee a bright career ahead of both of them. Many thanks also to our most recent lab partner, Alaa Moamer, someone with a solid training, generous and skilled, who is always ready for sharing knowledge or chatting on the latest findings of humankind. And I could not forget to thank also Halema Haiub, for often filling our work environment with good humor and optimism.

I would like to address special thanks to our nice 'neighbors', Nihad Tousson Abouelazm, Kwang-Bo Joung and Aurélie Tréfier Trindade, without whom many of my experiments would not have happened. Many thanks for all the help, for the antibodies and (not 'for all the fish' but) for the soups, snacks, and laughs.

Thank you to my co-supervisor, Dr. Gilles Gouspillou — a remarkable young scientist, always prone to innovative ideas and observations — and all his team.

Many thanks also to Dr. Marco Sandri and his team, brilliant minds behind *Mytho*, for the opportunity of such a fortunate collaboration and sharing precious insights — and a creative gene name as well.

Thank you to the members of the thesis committee: to Dr. John Di Battista, my academic advisor, always so kind and available, for his thoughts on the project; to Dr. Dilson Rassier, an authentic *gaúcho*, also for his availability and feedbacks on our project; and my special thanks to Dr. José A. Morais. His was the warmest *Luso-Canadien* welcome that Montreal has reserved for me. Amidst a major world setback during pandemic times, José and his family have gifted me with the priceless “home feeling” — *sentir-se em casa. Muito obrigado.*

My special thanks also to Drs. Maurilio José Pinto, Ana Lucia Fiebrantz Pinto and Vitor Last Pintarelli, outstanding examples of empathy merged to solid technical professionalism in healthcare. I am thankful for their guidance and support during and after my years at *Fundação de Apoio e Valorização do Idoso* (Curitiba, Brazil) and for all the opportunities given to me. Many thanks as well to Dr. Jonas Gurgel, an exceptional researcher, for his guidance and encouragement.

I address many thanks to the Division of Experimental Medicine, the Meakins-Christie Laboratories, and specially the Helen McCall Hutchison Foundation of the Division of Geriatric Medicine, and their respective staff, for their financial support and availability. I also appreciate the support from Canadian Institutes for Health Research through a grant to Drs. Hussain, Gouspillou and Sandri for the great project.

And finally, my deepest gratitude and love to my family. To my parents, Iara and Eduardo; my brothers, Fábio and Fernando; my sisters-in-law, Izabela and Priscila, and my beloved nieces and nephew, Julia, Fernanda e Matheus. I acknowledge a handful of best friends as well. You all are my main reason to look forward to better days. I apologize for the mistimed choice of faraway lands to venture out and feed my curiosities. Although I am physically distant today, having the privilege of your love and presence throughout life are my source of strength and motivation to get up every day, as a professional but mainly as a human being. *Muito obrigado.*

LIST OF ABBREVIATIONS

4E-BP1	Eukaryotic initiation factor-4E-binding protein-1
aa	Amino acids
AAV-shRNA-MYTHO	shRNA targeting MYTHO sequence
AAV-shRNA-Scramb	shRNA targeting scrambled sequence
AAV	Adeno-associated virus
AKT	Protein kinase B
AL	Autophagy-lysosome
AMP	Adenosine monophosphate
AMPK	AMP-activated protein kinase
AS	Alternative splicing
ATG	Autophagy-related gene
ATP	Adenosine triphosphate
ATPase	Adenosine triphosphatase
Atrogin-1/MAFbx:	Muscle atrophy F-box containing protein (<i>Fbxo32</i>)
BAX	Bcl-2-associated X protein
BCAS3	Breast carcinoma-amplified sequence 3
Bid	BH3 interacting-domain death agonist
BNIP3	Bcl2/Adenovirus E1B 19KDa interacting protein 3
BSA	Bovine serum albumin
C2C12	Mouse myoblasts cell line
Ca ²⁺	Calcium (ion, free)
Caspase	Cysteine-dependent aspartate-directed proteases
cDNA	Complementary DNA
CHF	Chronic heart failure
CHIP	Carboxyl terminus of Hsc70-interacting protein
CKD	Chronic kidney disease
CMA	Chaperone-mediated autophagy
COPD	Chronic obstructive pulmonary disease
COVID-19	Coronavirus disease 2019
DAPI	4',6-diamidino-2-phenylindole
DNA	Deoxyribonucleic acid
DNHP	2,4-dinitrophenylhydrazine
DPPC	Dipalmitoylphosphatidylcholine
E1	Enzyme activators of ubiquitin
E2	Enzyme conjugators of ubiquitin
E3	Ubiquitin ligases
ECL	Enhanced chemiluminescence
EDL	Extensor digitorum longus muscle
eIF2	Eukaryotic initiation factor 2
eIF3f	Eukaryotic translation initiation factor 3 subunit F
eIF4E	Eukaryotic initiation factor-4E
ER	Endoplasmic reticulum
Fbxo32	Atrogin-1 (gene), E3 ligase
FIP200	Focal adhesion kinase (FAK) interacting protein of 200 kDa
FoxO	Forkhead box protein O
GABARAP	Gaba type A receptor- associated protein
GABARAPL1	Gamma-aminobutyric acid receptor-associated protein
GAPDH	Glyceraldehyde-3-phosphate dehydrogenase

GAS	Gastrocnemius
GIM	GABARAP interaction motif
GSK-3 β	Glycogen synthase kinase 3 beta
HEK293	Human embryonic kidney 293 cells
HeLa	Immortalized cells line (Henrietta Lacks)
HSC70	Chaperone heat shock cognate 70 kDa protein
i.m.	Intramuscular
ICU	Intensive care unit
ICUAW	Intensive care unit-acquired weakness
IGF-1	Insulin-like growth factor 1
IR	Intron retention
KD	Knockdown
kDa	Kilo Daltons
KFERQ	Pentapeptide specific (aa) sequence/motif
KO	Knockout
LAMP2A	Lysosome-associated membrane protein type 2A
LC3	Microtubule-associated protein 1 light chain 3
LIR	LC3 interacting region
mRNA	Messenger RNA
mTOR	Mammalian target of rapamycin
mTORC1	Mammalian target of rapamycin complex 1
MuRF-1	Muscle-specific RING finger protein 1 (<i>Trim63</i>)
MUSA1	Muscle ubiquitin ligase of SCF complex in atrophy-1
Myh3	Embryonic myosin heavy chain
Myh8	Neonatal myosin heavy chain
MyHC	Myosin heavy chain
MyLC	Myosin light chain
MyoD	Myoblast determination protein 1
MYTHO	Macroautophagy regulator and youth optimizer
NF- κ B	Nuclear factor kappa-light-chain-enhancer of activated B cells
NMD	Nonsense-mediated mRNA decay
Npl4	Nuclear protein localization protein 4
orf	Open reading frame
p70-S6K	p70 ribosomal protein S6 kinase beta-1
p97	Valosin-containing protein (ATPase)
PBS	Phosphate buffer saline
PBST	Phosphate buffer saline added Tween®20 detergent
PCR	Polymerase chain reaction
PE	Phosphatidylethanolamine
PI-3K	Phosphatidylinositol 3-kinase pathway
PI3KC3	Class III phosphatidylinositol 3-kinase
PI3P	Phosphatidylinositol-3-phosphate
pre-mRNA	precursor mRNA
PVDF	Polyvinylidene difluoride
RNA	Ribonucleic acid
RNAi	RNA interference
ROS	Reactive oxygen species
RT-PCR	Reverse transcription-PCR
S6K1	Ribosomal protein S6 kinase 1
SDH	Succinate dehydrogenase

SDS-PAGE	Sodium dodecyl sulphate polyacrylamide gel electrophoresis
SEM	Standard error of the mean
SERCA	Sarco (endo) plasmic reticulum Ca ²⁺ -ATPase
shRNA	Short hairpin RNA
SMART	Specific of muscle atrophy and regulated by transcription
siRNA	Small interference RNA
SOD	Superoxide dismutase
SQSTM1	Sequestosome 1 (p62)
SR	Sarcoplasmic reticulum
STIM1	Stromal interaction molecule 1
SV	Splicing variants
TA	Tibialis anterior
TEM	Transmission electron microscopy
TNF- α	Tumor necrosis factor alpha
Trim63	MuRF-1 (gene), E3 ligase
Ufd1	Ubiquitin recognition factor in ER associated degradation 1
ULK1	Uncoordinated-51-like-kinase complex 1
UP	Ubiquitin-proteasome
UVRAG	UV radiation resistance-associated gene protein
VPS	Vacuolar protein sorting
VPS15	Vacuolar protein sorting 15
VPS34	Phosphatidylinositol 3-kinase VPS34
WD	Dipeptide, tryptophan-aspartic acid (W-D)
WD40	Protein domain (~40aa) terminating in WD
WIPI	WD repeat domain interacting with phosphoinositides
WT	Wild type

CONTRIBUTION OF AUTHORS

This thesis was prepared according to principles outlined in McGill University's "Guidelines for Thesis Preparation". The format conforms to "traditional monograph thesis" option. The contributions of each author are outlined below.

Felipe E. Broering, MD (FEB): This thesis was written by M.Sc. candidate FEB, who performed literature review, prepared and revised this document. FEB optimized several laboratory experiments, performed immunoblotting and immunohistochemistry, and assisted with animal experiments, AAVs injections, harvesting and processing of tissues, qPCR, immunofluorescence, transmission electron microscopy and data analysis. FEB attended research team meetings, presented preliminary research findings to the Meakins-Christie Laboratories meetings and to the M.Sc. Thesis Committee meetings.

Sabah N. A. Hussain, MD, PhD (SNAH): Thesis supervisor. SNAH regularly provided mentorship, guidance and support for all experiments and sections of this thesis. SNAH also provided supportive environment for achieving this thesis objectives, attended to all committee meetings, and provided extensive feedback and direction on this thesis.

Gilles Gouspillou, PhD (GG): Thesis co-supervisor. GG provided mentorship, guidance and inputs for all sections of this thesis.

Jean-Philippe Leduc-Gaudet, PhD (JPLG): Former Ph.D. fellow at Dr. Hussain's laboratory and currently postdoctoral fellow in Dr. Sandri's laboratory at University of Padova. JPLG regularly provided mentorship, guidance and support for all experiments and extensive feedback on all sections of this thesis.

Dominique Mayaki, MSc (DM): Research assistant. DM provided technical expertise and assisted with qPCR and mRNA detection.

Laurent Huck, PhD (LH): Research associate. LH provided technical expertise and assisted with animal experiments, preparing muscle sections and immunostaining.

Marco Sandri, MD, PhD (MS): Research collaborator. MS provided many insightful comments and suggestions on the study design and methodology.

José A. Morais, MD (JAM): Member of the M.Sc. thesis committee. JAM attended all committee meetings and provided insightful comments and suggestions on the study design.

Dilson Rassier, PhD (DR): Member of the M.Sc. thesis committee. DR attended all committee meetings and provided insightful comments and suggestions on the study design.

Giovanni (John) A. Di Battista, PhD (JADB): Academic advisor member of the M.Sc. thesis committee. JADB attended all committee meetings and provided insightful comments and suggestions on the study design.

SECTION 1: INTRODUCTION AND LITERATURE REVIEW

1.1. Introduction

The mammalian muscular system is composed of three types of muscles: skeletal, cardiac, and smooth muscles. The skeletal muscle, a specific type of striated muscle tissue, is a heterogeneous collection of specialized cells, myofibres, grouped within connective tissue (1). In humans, skeletal muscles account for around 40% of the body mass, 60% of the body's protein stores, and are mainly responsible for breathing, movement, postural support, heat maintenance and are a central component of the body's metabolism (2).

The combination of loss of muscle mass and strength is a common clinical feature found in a variety of acute or chronic, and often overlapping, conditions: diabetes, cancer cachexia, chronic kidney disease (CKD), infections, weakness related to critical illness, neuromuscular disorders, chronic heart failure (CHF), disuse, microgravity and age-related muscle wasting represent some of the many phenotypes (3-5). It is a major challenge to address the prevalence and healthcare costs of muscle atrophy as a general condition. Attempts to estimate its prevalence can widely range from 5% up to 50% as it is directly proportional to age and, certainly, sarcopenia is a key factor that gives rise to muscle atrophy in general (6). Although recent consensus definition of sarcopenia (2-5) differs from the largely accepted definition of the age-related decline in lean body mass (7), in the final analysis, loss of skeletal muscle mass and strength bring tremendous biopsychosocial consequences on quality of life and associated morbidity and mortality. A meta-analysis and systematic review, with 58,404 individuals over 60 years old, found an overall prevalence of loss of muscle mass in the world of 10% (8). Direct healthcare costs and indirect socio-economic implications are markedly high. In the USA, public health costs with sarcopenia were \$18.5 billion, occupying nearly 1.5% of total healthcare budget in the year 2000 (6, 9). A recent systematic review demonstrated a trend toward a more important use of healthcare resources in the sarcopenic population world wide

(10). However, due to the heterogeneity of the studies investigated—among other biases, the definition of sarcopenia itself on each one of those studies analyzed is fairly a matter of discussion (11), there is still a great demand for more precise assessments on the topic regarding economic analysis. Another major cause of muscle atrophy is CKD, the prevalence of this condition, only in Canada, was around 3 million adults in 2009 (12); in the USA, approximately 20 million in 2003 (13) and muscle atrophy occurs virtually in the totality of these individuals, regardless of the age. In addition, individuals suffering from CHF show an increased prevalence of loss of muscle mass and muscle function, and in older adults with CHF the prevalence can reach up to 20% (14). Other important examples of muscle wasting conditions worth to mention, with special interest since the surge of the coronavirus disease 2019 (COVID-19) pandemic, are the intensive care unit-acquired weakness (ICUAW) and COVID-19 itself. ICUAW occurs in critically ill patients resulting in sustained impairment long after the intensive care unit (ICU) stay, and as much as 40% of critically ill patients may experience this condition (15). Moreover, COVID-19 long-term consequences are beginning to be clarified but it has been already demonstrated that it can affect directly and indirectly mainly the cardiorespiratory and neuromuscular systems, as well as mental health (16). Particularly in older adults, the isolated feature of intense myalgia on hospital admission due to COVID-19 is shown to be associated with abnormal lung images and poor outcomes (17). The pathophysiology of muscle injury in COVID-19 is attributable to many factors like cytokine storm, disease severity, mechanical ventilation, prolonged ICU stays, malnutrition, myotoxic drugs and polypharmacy. But the precise mechanisms, even in milder cases, as well as the long-term sequelae of the direct effects of coronavirus in the muscle cells of disease survivors remain unclear (17). Ultimately, skeletal muscle health and muscular homeostasis are important determinants of quality of life and longevity, with major socio-economic impacts at the individual, family and community levels. Skeletal muscle loss and its functional consequences

constitute a serious public health issue. Efforts to mitigate the underlying conditions should be an essential item of public health policies world wide.

On the other hand, translating basic scientific research to clinical practice, and to public health gains, constitute another important and major challenge in the biomedical research. Although there is still a gap of knowledge on several relevant issues in the field of skeletal muscle dysfunction, much progress has been achieved. In this sense, autophagy is an essential biological process involved in skeletal muscle health and disease that has been intensively investigated. Skeletal muscle mass is regulated by the balance between protein synthesis and protein degradation, and autophagy is among four pathways which are responsible for protein degradation inside skeletal muscle fibres. It is an intracellular degradation process by which proteins, organelles, and other cytoplasmic structures are engulfed into vesicles, delivered to lysosomes, and eventually digested and recycled (18, 19). A tight regulation of autophagy is essential for the maintenance of homeostasis, so that insufficient or excessive organelles degradation do not result in undesirable cellular damage and tissue dysfunction (19, 20). Over the last decades, despite many progresses on the discovery of autophagy-related genes, much remains unrevealed. Better knowledge on autophagy and its regulation in the skeletal muscle tissue may represent the possibility of novel diagnostic and overall therapeutic approaches for many conditions.

Our laboratory has an active cooperation with Dr. Marco Sandri's research group (University of Padua, Italy) for the past several years. A few years ago, that group investigated the functional importance of FoxO transcription factors in regulating skeletal muscle atrophy by generating transgenic mice with muscle selective deletion of FoxO1, FoxO3, and FoxO4 transcription factors (FoxO^{1,3,4} KO). Sandri's group compared muscle gene expression elicited by acute starvation in wild type (WT) and FoxO^{1,3,4} KO mice (21). They reported that FoxO^{1,3,4} KO mice are resistant to starvation-induced atrophy and that FoxO transcription factors control

several stress-response pathways. Such findings represent major breakthroughs in our overall understanding of the regulatory importance of FoxO in muscle autophagy, but many of their transcriptional targets, upstream regulators, and interacting partners remain to be elucidated. Sandri's group identified one FoxO-dependent protein whose expression was upregulated in skeletal muscles of WT mice but not in FoxO^{1,3,4} KO mice in response to acute starvation: a protein encoded by *D230025D16Rik* gene in mice and *C16orf70* in humans. During the preparation of this thesis, two relevant *in vitro* studies addressed this novel gene (22, 23) and despite important advances, much remains to be clarified about the function and expression of this gene. In our particular interest, in skeletal muscles.

This thesis is focused on describing the phenotype of D230025D16Rik knockdown (KD) in the mouse skeletal muscle. The possible importance of this protein, designated as MYTHO, in the regulation of skeletal muscle mass, autophagy and contractile function will be discussed.

1.2. Skeletal muscle: structure and classification

The skeletal muscle is a heterogeneous collection of specialized cells called myofibres, grouped within sheaths of connective tissue (1). It is a type of striated muscle tissue where mature myofibres develop through fusion of myoblasts, the muscle precursor cells, giving it its multinucleated characteristic (24). The highly organized structure of the myofibres gives to the tissue the striated characteristic, each of the myofibres contain a high concentration of myofilament proteins, organized into myofibrils within the sarcoplasm. The myofibrils are composed of a recurrent histological pattern called sarcomere, the basic contractile unit of skeletal muscles. These structures are separated from each other by dark lines, the Z disks. Contraction, at the basic unit level, occurs through a highly organized and reversible coupling between the myofilament proteins, actin and myosin. The sarcoplasmic reticulum (SR) and

mitochondria surround the myofibrils, as well as other essential organelles to contractility and cell survival (1).

There are 3 types of muscles in mammals, skeletal, cardiac and smooth muscles. A mixture of fibre types is found in skeletal muscles, which can be classified based on structural and functional aspects. They are categorized based on the subtypes of myosin heavy chain (MyHC) that they express. In mouse muscles, four major fibre types with distinct MyHC composition are found: type I, IIA, IIB, and 2X. These subtypes are classified as slow-twitch (type I) or fast-twitch (type IIA, IIB and 2X) based on the velocity of the fibre shortening on contraction (24, 25). Slow-twitch muscle, with a denser capillary network and rich in myoglobin, mitochondria and oxidative enzymes, are specialized to perform continuous activity, also called red muscles. While fast-twitch muscle, with fewer mitochondria and myoglobin, are characterized by a glycolytic metabolism and specialized for phasic activity, identified in general with white muscles (24).

Slow-twitch fibres develop a lower contractile force relative to fast-twitch fibres, but the contraction may be maintained for a longer period. Therefore, the higher the oxidative capacity, the more fatigue-resistant the fibre. The type IIA fibres, however, which contain high concentration of mitochondria and capillaries but are also rich in glycolytic enzymes, are classified as oxidative glycolytic fibres. This metabolic capacity gives them a dual characteristic, fast and fatigue resistant (24, 26). In human, type IIX fibres are not only the skeletal muscle fastest fibres as well as the most easily fatigued, they rely mostly on glycolytic metabolism (26). Though not expressed in humans, type IIB fibres are the fastest of the four isoforms and they are found in muscles of small mammals such as rodents (24, 26).

1.3. Regulation of skeletal muscle mass

Skeletal muscle mass is controlled by a balance between protein synthesis and protein degradation. Under healthy conditions, progressive exercise training and adequate nutrition, for example, can result in a net gain in protein synthesis, increasing the size of the pre-existing muscle fibres, promoting hypertrophy (27). By contrast, atrophy is the result of muscle protein loss when protein degradation exceeds protein synthesis, decreasing the size of the pre-existing fibres, a very common issue in clinical practice. Such findings may be observed in various catabolic states, including acute or chronic conditions like sepsis, cachexia, heart failure, chronic obstructive pulmonary disease, renal failure, AIDS, neuromuscular disorders, prolonged bed rest and ageing (5, 27).

1.3.1. Protein synthesis

The most important pathways that promote skeletal muscle protein synthesis are the AKT/FoxO transcription factor pathway and the mammalian target of rapamycin complex 1 (mTORC1) pathway. *In vitro* and *in vivo* studies have identified protein kinase B (AKT) a serine/threonine kinase, as a crucial regulator of protein synthesis in both hypertrophy and atrophy conditions (28, 29). The energy status of the cell, the high extracellular availability of amino acids, glucose and other nutrients are important regulators of these pathways. It is well established that growth-promoting stimuli such as insulin and insulin-like growth factor 1 (IGF-1) activate AKT through the phosphatidylinositol 3-kinase pathway (PI-3K) (28). Active AKT phosphorylates glycogen synthase kinase 3 beta (GSK-3 β), releasing its inhibition of an essential factor for protein synthesis, the eukaryotic initiation factor 2 (eIF2) (30, 31). AKT also phosphorylates and inactivates FoxO transcription factors (like FoxO1, FoxO3 and FoxO4) and keep them in the cytosol through direct interaction with the docking protein 14-3-3 (32). In addition, AKT activates mTORC1, another important nutrient-sensing kinase,

resulting in the promotion of protein synthesis, cell growth and proliferation. mTORC1 activates the ribosomal protein S6 kinase beta-1 (p70-S6K) and inhibits translation of initiation factor 4E-binding protein 1 (4E-BP1), thereby releasing the inhibitory effect of 4E-BP1 on protein synthesis (31, 33).

1.3.2. Protein degradation

Under catabolic conditions, there is a state of enhanced skeletal muscle proteolysis, which can be beneficial in the early phases of acute illnesses, as free amino acids provide other tissues with substrates for vital cellular processes (34, 35). However, sustained protein degradation in either acute or chronic conditions results in muscle atrophy, such as in sepsis, trauma, cancer, diabetes, disuse, COPD, cardiac and renal failure, leading to increased severeness of disease (5). Loss of muscle mass in these various disease states is mostly due to the breakdown of contractile proteins (36, 37). There is also evidence that these chronic conditions are also associated with a prolonged inhibition of IGF-1/PI-3K/AKT pathway inside skeletal muscle fibres which triggers the removal of the inhibitory effect of this pathway on FoxO transcription factors. Activation of these factors leads to transcription upregulation of two muscle-specific ubiquitin E3 ligases (*Trim63* and *Fbxo32*), important enzymes involved in the process of recognition of protein substrates to be degraded, and several other autophagy-related genes (38, 39). Muscle protein degradation is regulated by four pathways: the calpains, the caspases, the ubiquitin-proteasome (UP) and the autophagy-lysosome (AL) pathways. The first three are responsible for degradation of myofilament proteins while the AL pathway is primarily responsible for the degradation of long-lived cytoplasmic proteins and organelles (35, 40).

Among many other functions, the calpains and caspases pathways are essential for skeletal muscle proteolysis as they can disrupt the rigid structure of the contractile apparatus

(41, 42). Calpains are Ca^{2+} -dependant cysteine proteases activated in response to sudden increases in intracellular Ca^{2+} concentration (43). These enzymes have their conformation changed by Ca^{2+} and this will activate a catalytic domain, giving them the property of cleaving specific proteins (41). In myofibres, three main calpain isoforms can be detected including m-calpain and μ -calpain (universally expressed), and the muscle-specific, calpain 3 (41). These enzymes release myofilament proteins by cleaving the sarcomeric components responsible for structural integrity of the contractile unit, like titin and nebulin (44). Under normal conditions, calpains are mostly inactive and are tightly regulated by an endogenous inhibitor, calpastatin (43). In acute disease states or in response to cellular damage, calpains are activated providing the cell immediate availability of metabolic substrates; however, a sustained activation of this pathway can lead to unregulated proteolysis, generalized tissue damage, and cell death (44, 45). The role of the calpains have been confirmed under different modes of stress in skeletal muscle. In sepsis, for example, studies have documented increased calpain activity as an important consequence of reduced activity of the calpains inhibitor, calpastatin (46) and such condition greatly contributes to the decline in force-generating capacity (47). Disuse and rehabilitation models showed overexpression of muscle-specific calpastatin and slow the progression of muscle wasting (48) but also the calpains role in skeletal muscle remodelling due to exercise training (49). More recent evidence suggests that calpains have many other functions in skeletal muscle fibres including regulation of cell signalling by altering specific protein biological function. For example, they influence mitochondrial function by generating calpain-truncated proteins, like the calpain-mediated cleavage of the BCL-2 family member, Bid, resulting in its truncated form known as tBid. In cardiac myocytes, tBid can translocate to the mitochondria and recruit Bcl-2-associated X protein (BAX), leading to permeabilization of the mitochondrial membrane and increased reactive oxygen species (ROS) production. They

also contribute to membrane repair in skeletal muscles and are involved in the conformation of triad junctions (50).

The cysteine-aspartate proteases, known as the caspases, are another family of enzymes with an important role upstream of the UP pathway. Caspases are mainly activated during the process of apoptosis, where they contribute through a series of proteolytic cleavages to break up the structural and functional elements of the cell (42). Insulin-resistance and cytokine upsurges are present in many catabolic states, and activate apoptotic and caspase pathways in different tissues, including skeletal muscle (51, 52) Caspase 3, the terminal protease in the caspase pathway, contributes mainly to nuclear apoptosis. Activation of caspase 3 has been described in different skeletal muscle wasting conditions such as cancer cachexia, ventilator-induced muscle weakness, and neuromuscular disorders (53-55). In addition, denervation-induced muscle atrophy was prevented by caspase 3 knockout (56). Nonetheless, myofibres are multinucleated cells, and caspase 3 activities may be insufficient to induce cell death. In this regard, by cleaving contractile proteins, caspases may contribute to myofibre remodelling and myofibre weakness (57). In addition, caspase-cleaved actin fragments have been found in atrophying muscles of diabetes and chronic uremia animal models (51). Altogether, these evidence suggest that caspase 3 activation may lead to contractile dysfunction in skeletal muscle in different catabolic conditions. Although not the focus of our study, it is opportune to emphasize the importance of such findings on protein degradation, aiming to explore more this field in prospective analyses.

1.4. Ubiquitin-proteasome pathway

The UP pathway is a system dedicated for proteolysis of a variety of proteins and it is commonly accepted as the main proteolytic system targeting myofibrillar proteins (58, 59). It is characterized as an adenosine triphosphate (ATP)-dependant pathway, composed of two

distinct and successive phases: covalent addition of ubiquitin to the target proteasomal substrates and degradation of the tagged substrate by the 26S proteasome (60). This process of tagging proteins destined for the proteasome is known as ubiquitination and requires a sequential action of three enzymes. First, ubiquitin is catalyzed, in an ATP-dependant way, by the E1-ubiquitin activating enzymes. This activated ubiquitin molecule is then transferred to the E2 ubiquitin-conjugating enzymes, that transports ubiquitin to the E3 ubiquitin-ligating enzymes. The E2-E3 enzyme pair will determine what type of protein the ubiquitin machinery is targeting. The E3 ligases will add covalently ubiquitin to lysine residues (K48), the most abundant ubiquitination site, of targeted proteins (61). The process is replicated until the substrate contains a tetramer of ubiquitin as the minimum signal for efficient targeting (62, 63), and the polyubiquitylated protein is ready to be recognized and degraded by the proteasome (35) — although some studies have been challenging this paradigm more recently, as monoubiquitination was revealed as having proteolytic roles as well (64, 65).

The 26S proteasome responsible for the degradation phase is composed of a proteolytic cylindrical core, 20S, and two regulatory caps, 19S protein complex. The 19S caps recognizes, binds the ubiquitin-tagged proteins, and eventually removes the ubiquitin chain before the translocation of the substrate to the 20S core. To promote the substrate translocation into the core, the 19S caps employs ATPase activity to unfold the target protein and opens the central channel. Inside the 20S proteasome, substrates are cleaved into small peptides by the 20S core subunits. These oligopeptides are then released to the cytoplasm to be finally degraded into free amino acids by other peptidases (35, 58).

In skeletal muscles, it has been reported that two main E3 ligases are significantly upregulated in several models of muscle atrophy (35, 66, 67). One of these two ligases is known as Muscle Atrophy F-box containing protein (MAFbx/Atrogin-1) which is encoded by the *Fbxo32*, and the second E3 ligase is known as Muscle RING Finger containing ligase (MuRF-

1) and is encoded by *Trim63* gene (66). In mice lacking *Fbxo32* or *Trim63*, it was possible to prevent denervation-induced muscle atrophy, indicating their critical roles in this model of muscle atrophy (66). Both ligases execute very similar catalytic reactions, but they have different protein targets. For instance, Atrogin-1 targets especially MyoD protein, which is a master regulator of myoblast differentiation, and eIF3f protein, which is involved in protein synthesis (68, 69). MuRF-1 selects mainly sarcomeric proteins such as titin, myosin light chain (MyLC) and MyHC (70-72).

Different catabolic stimuli can trigger activation of skeletal muscle proteasome activity. For instance, oxidative stress seems to have an important role, as mouse myoblasts exposed to elevated levels of ROS had significant activation the proteasome and upregulation of ubiquitin, E2 activating and E3 ligating enzymes (73). In rat myotubes, hypoxic stress also activates the proteasomal degradation of myofilaments and upregulation of *Fbxo* ligase (Atrogin-1) (74). Finally, pro-inflammatory cytokines particularly, tumor necrosis alpha (TNF- α) strongly activates proteasome activity and triggers significant upregulation of *Trim63* and *Fbxo32* expressions through the nuclear factor kappa-light-chain-enhancer of activated B cells (NF- κ B) pathway activation (75, 76).

1.5. Autophagy-lysosome pathway

The two major pathways by which protein degradation occurs in eukaryotic organisms are the UP and the AL pathways. Autophagy is a well conserved process throughout evolution by which cells can break down and recycle organelles, bulk portions of cytoplasm and long-lived proteins (18, 77). There are two main phases in this pathway where cytosolic material is first delivered to the lysosomal lumen and then, degraded by lysosomal enzymes (40). At basal levels, intracellular homeostasis is maintained through a number of processes and autophagy has a central role, preventing the accumulation of damaged and dysfunctional organelles and

proteins (18). However, in response to a myriad of stimuli such as microbial pathogens, cellular stress and nutrient deprivation, it can be promptly activated far above normal levels (19). To achieve and maintain homeostasis, autophagy must be tightly regulated, as insufficient or excessive degradation of cytoplasmic components can be highly deleterious to the cell (19).

There are three main classes of autophagy known in mammalian cells: microautophagy, chaperone-mediated autophagy (CMA) and macroautophagy. In microautophagy, small cytosolic portions are engulfed by the lysosome, the microautophagic vesicle membrane is degraded and its content, digested by hydrolases (78). The level of microautophagy, however, as well as its role in skeletal muscle remain largely unknown (18, 20). CMA targets soluble cytosolic proteins, acting on substrates with a specific pentapeptide sequence, KFERQ (18, 19, 79, 80). The chaperone-substrate complex interacts with the lysosomal-associated transmembrane protein 2A (LAMP2A), leading to protein unfolding and translocating them into the lumen, where they are digested by the lysosomal hydrolases (81). Many cellular stressors as prolonged starvation, exposure to cytotoxic substrates and oxidative stress can strongly induce CMA, and failure to activate this type of autophagy may lead to accumulation of dysfunctional proteins (81). Nevertheless, it is not well established the real contribution of CMA in skeletal muscle loss and homeostasis (18, 20).

The main type of autophagy in skeletal muscle is macroautophagy, often referred as autophagy. This pathway targets organelles, protein aggregates and other long-lived cytoplasmic components for degradation in the lysosome (18, 19). The transport of the substrates to the lysosome is done by double-membrane vesicles, the autophagosomes (82). The process is highly inducible in response to any sort of stress, acting primarily as a protective mechanism (19, 82, 83). Autophagy responds to environmental signals through a tight-regulated process which involves the expression of several autophagy-related genes (ATGs)

(83). ATGs were first described in yeast, but it led to the detection of their orthologs in higher eukaryotes (84).

Autophagy is initiated by the uncoordinated-51-like-kinase (ULK1) complex 1. This complex is under positive control of the AMP-activated protein kinase (AMPK) pathway and negative control by the mTORC1 pathway (85). mTORC1, a nutrient-sensing kinase, is regulated by several cues, amino acids, glucose, and other cell energy status, and promotes protein synthesis, cell growth and cell proliferation (86, 87). AMPK responds to modifications in the intracellular AMP/ATP ratio, also working as an energy sensor (82, 88). The interaction of proteins ULK1, ATG13, FIP200 and ATG101 leads to formation of the ULK1 initiation complex and the integration of inhibitory or stimulatory signals received from mTORC1 and AMPK will respectively determine its activity (18, 82, 85). Under nutrient abundant conditions, mTORC1 phosphorylates and inactivates ULK1 complex by acting in multiple serine residues and thereby prevents its interaction with AMPK, and the result is the inhibition of autophagy (85, 89). Under nutritional distress or starvation, with high levels of AMP and low levels ATP, AMPK is activated and removes mTORC1 from the ULK1 complex (85, 90). Such dissociation activates ULK1, which phosphorylates ATG13 and initiate autophagosome formation (82). After this first process, the autophagosome biosynthesis occurs through the phases of nucleation, elongation and maturation (83). The nucleation phase is characterized by the phagophore formation, a double membrane vesicle that elongate (91). A critical component at this stage is the BECLIN1 complex, formed by the interaction of class III phosphatidylinositol 3-kinase (PI3KC3), VPS15, UVRAG, ATG14L and BECLIN1 protein (92). This complex assembly activates PI3KC3 to increase the production of phosphatidylinositol-3-phosphate (PI3P) and these phospholipids recruit additional ATG proteins required for the autophagosome formation (77, 93).

The next step is the elongation of the pre-autophagosome, promoted by two ubiquitin-like conjugation systems. Where LC3 and ATG12 act as ubiquitin-like molecules, while ATG7 and ATG10 enzymes, respectively, act as E1-like and E2-like enzymes (94). In the first pathway, ATG7 enzyme activates ATG12. Then, ATG10 couples ATG12 to ATG5, leading to the formation of a dimeric conjugate which binds to ATG16L protein (94, 95). The newly formed trimeric complex is translocated to the phagophore and will work on the membrane elongation (94). The second conjugation pathway requires the microtubule-associated protein 1 light chain 3 (LC3), initially as its intact precursor, pro-LC3. The cysteine protease ATG4 cleaves the precursor creating its cytosolic form: LC3B-I. Then, LC3B-I is conjugated with phosphatidylethanolamine (PE) through ATG7, ATG3, and the ATG16L complex. This process is known as the lipidation of LC3-I, producing LC3B-II, which is translocated to the phagophore and is integrated to the expanding membrane (94, 96). After its complete formation, most of the proteins required for the autophagosome nucleation and elongation are separated from the vesicle, but LC3B-II persists in its association with the mature autophagosome (97, 98). Because of its integration into autophagosome membrane, LC3B-II protein is widely accepted as a marker of autophagosome formation (96, 98, 99). Following its completion, the autophagosome is transported through microtubules to the centrosome, a compartment where the lysosomes are concentrated (100). The autophagosome docks and fuses with the lysosome generating the autolysosome (94, 97). This is the maturation phase, where the cargo is digested into monomers by lipases, proteases and nucleases. Eventually, the degraded products are recycled back into the cytoplasm, providing the cell with vital substrates (101).

1.6. Autophagy and skeletal muscle function

All eukaryotic cells require basal levels of autophagy to sustain homeostasis and can dramatically upregulate this process in response to cellular stress to various degrees (77). Muscle wasting is common finding in clinical practice, and both the UP and the AL pathways are greatly increased in atrophying muscles. As previously described, the activation of these pathways is finely modulated by a complex network involving the FoxO transcription factors (40). Autophagy at basal levels is an essential process for maintaining muscle mass and its functional properties (102).

The generation of mice with muscle-selective deletion of *Atg7* gene revealed several morphological abnormalities that are associated with inhibition of muscle autophagy. These include decreased myofibre size, misalignment of the sarcomeric Z-bands, and the accumulation of damaged organelles and protein aggregates (20). There are also functional consequences of *Atg7* deletion in skeletal muscles including decreased absolute and specific force-generating capacity (21). It has also been reported that muscle-selective deletion of autophagy triggers a compensatory upregulation of the proteasome proteolytic activity (20). As this pathway cannot degrade those protein aggregates and organelles, over activation of UP pathways could not rescue the phenotype (21). By preventing an increase in oxidative damage, and inhibition of apoptosis, basal muscle autophagy contributes to the survival of myofibres. This protective role can be partially explained by the recycling of damaged and damaged organelles and proteins aggregates (102).

Various murine models of muscle atrophy have been used to study the relationship between atrophy and autophagy. Denervation models are quite effective in generating loss of muscle mass, followed by a marked reduction in mitochondrial content as well as an increase in mitochondrial dysfunction, particularly augmented ROS production, compromised respiration and increased permeability (103, 104). Findings that could be explained, at least in

part, by a rapid activation of the autophagy pathways in general and selective removal of dysfunctional mitochondria by the autophagy pathway (mitophagy) (104-106). Sepsis models can also induce dramatic muscle wasting, loss of function, and adaptations in mitochondrial bioenergetics (107). Sepsis triggers a decrease in the mitochondrial respiration rates in limb and ventilatory muscles, and reduction in the levels of the electron transport chain subunits (108-110). Importantly, clinical studies have shown that sepsis-induced mitochondrial dysfunction is related to disease severity and patient survival (111, 112). In addition, Mofarrahi et al reported significant morphological abnormalities in muscle mitochondria associated with dysfunctional opening of the permeability transition pores and reduced mitochondrial biogenesis (113). These abnormalities were associated with induction of the autophagic flux, increased number of autophagosomes, enhanced LC3B protein lipidation, and upregulation of several autophagy-related genes such as *LC3B*, *BECLIN-1*, *PI3KC3*, *LAMP2A*, *ATG14L*, *ATG4B* and *ATG12*. These results suggest that mitophagy is essential recycling mechanism of damaged mitochondria in skeletal muscles of septic mice (113). Another model in which skeletal muscle atrophy is associated with increased autophagy, and upregulation of several autophagy-related genes, is acute starvation. Studies have shown a significant increase in the autophagosome formation and LC3B lipidation in skeletal muscle of acutely starved mice (39, 114). Moreover, this model exemplifies an intriguing characteristic of skeletal muscle autophagy, namely, that although acute starvation elicits transient activation of the autophagy pathway in most tissues, lasting only a few hours, in skeletal muscle the autophagic flux can be detected days after the acute starvation (40, 114).

As any other biological process, there is an optimal level of autophagy in order to maintain homeostasis. Autophagy has been demonstrated as an essential evolutionary mechanism in the clearance of damaged organelles and its balance is tightly regulated. An exaggerated removal of cytoplasmic contents results in dramatic loss of skeletal muscle mass,

as well as an insufficient activation of the autophagic activity may lead to an excessive accumulation of damaged organelles, uncontrolled cellular injury and tissue dysfunction (19, 20, 40, 102). Altogether, these data support strong evidence of the importance of autophagy in regulating muscle mass balance in healthy and atrophying skeletal muscle.

1.7. FoxO transcription factors and MYTHO

Some members of the FoxO family of transcription factors (FoxO1, FoxO3a, FoxO4) have been identified as key regulators of the activity of the ubiquitin-proteasome and the AL pathways. These two pathways are involved in the breakdown of myofilaments and recycling of damaged organelles (39, 40). Specifically, FoxO transcription factors regulate the expression muscle-selective ubiquitin E3 ligases *Trim63* (MuRF1) and *Fbxo32* (Atrogin-1) expression, collectively referred as ‘atrogenes’ (27, 38). The expression of these two E3 ligases increase significantly in several catabolic conditions such as and starvation, uremia, denervation, amyotrophic lateral sclerosis, cancer, and immobilization (27, 38, 115). Other transcription factors that are also involved in MuRF1 expression including NF- κ B (76). FoxO1 inhibits the inhibitory effect of IGF-1 on *Fbxo32* expression leading indirectly to upregulation of *Fbxo32* (29). In addition, FoxO3a directly binds to the *Fbxo32* promoter and increases its transcription in mouse skeletal muscles (38) and blocking FoxO3a activity prevents the induction of *Fbxo32* expression during starvation or corticosteroid administration (116). With respect to FoxO4, there is evidence that it enhances *Fbxo32* expression in response to TNF- α exposure *in vitro* (117). Moreover, TNF- α -induced activation of FoxO1 and upregulation of *Fbxo32* upregulation occur concomitantly with AKT inhibition (29, 32). Altogether, these data indicate that the FoxO family regulate and are regulated at variable degrees, by catabolic and anabolic signals.

In normal muscle, FoxO transcription factors are phosphorylated by AKT and remain bound to 14-3-3 proteins in the cytosol. Disruption of phosphorylation triggers mobilization to the nucleus, where FoxO factors transcribe several autophagy-related genes. It has been reported that FoxO transcription factors co-ordinately activates the autophagic and proteasomal pathways in ventilatory and limb muscles (39, 118, 119). FoxO transcription also regulates several rate-limiting proteins associated with these pathways, including LC3, p62/SQSTM1, BECLIN1, ATG12, GABARAPL1, BNIP3 and Fbxo32 (38, 39, 120).

Sandri's group investigated FoxO-dependent atrogenes by comparing gene expression in skeletal muscles of WT mice undergoing muscle atrophy mediated by starvation to those expressed in skeletal muscles of mice with the muscle-selective FoxO^{1,3,4} KO (21). They reported that FoxO^{1,3,4} KO mice are resistant to starvation-induced atrophy and that FoxO transcription factors control several stress-response pathways such as unfolded protein response, ROS detoxification, and DNA repair and translation. They also found that the expression of two ubiquitin E3 ligases (MUSA1 and SMART) is regulated by FoxOs inside muscle fibres.

To identify novel proteins that regulate autophagy, Sandri's group compared the transcriptomes of limb muscles of WT and FoxO^{1,3,4} KO mice exposed to 24 hours of acute starvation (unpublished results). Their analysis was focused on novel transcripts that have an open reading frame (orf), conserved across species, and have autophagy related LC3-interacting regions (LIRs) or GABARAP interaction motifs (GIM) in the coding sequence. They identified one FoxO-dependent candidate, that was upregulated in skeletal muscles of WT mice but not in FoxO^{1,3,4} KO mice. This candidate is *D230025D16Rik* and the ortholog is annotated as *C16orf70* in humans. Based on pilot studies performed in the nematode *Caenorhabditis elegans*, they found that this protein is somehow involved in the autophagy regulation and promotes survival, therefore named MYTHO (Macroautophagy regulator and

YouTH Optimizer). Bioinformatic analyses of the protein structure suggest that it may interact directly with WIPI2 protein, which is a protein required for the autophagosome formation. Further analysis also confirmed that MYTHO is indeed a highly conserved gene across species.

Our assessment of *D230025D16Rik* gene expression using *Ensembl* (<https://ensembl.org/>) (121) revealed that two of the six reported *MYTHO* mRNA splicing variants (SV) have the same transcript type protein coding: mRNA D230025D16Rik-201, which encodes for a 47-48 kDa protein (Isoform-201) and a shorter one, mRNA D230025D16Rik-203, that encodes for a 13 kDa protein (Isoform-203). The other four mRNA SV are: mRNA D230025D16Rik-202 and mRNA D230025D16Rik-205, both with same type of transcript, nonsense-mediated mRNA decay (NMD); and mRNA D230025D16Rik-204 and mRNA D230025D16Rik-206, both having intron retention (IR) as mode of splicing. Importantly, our preliminary analysis of the expression of these isoforms in C2C12 myoblasts using selective PCR primers revealed that the isoform 203 is relatively not as abundant, only 4% comparing with the other SV with the same mode of splicing, isoform 201. Therefore, we focused our studies on the Isoform-201, encoding a 47-48kDa protein. Other databases reported this protein as one of unknown function but conserved throughout eukaryotes, that the human ortholog, C16orf70, localizes in nuclear speckles and Golgi apparatus, and that it is expressed in all tested cell types (22). Very recently, while the preparation of our work, an ortholog of human C16orf70, KinkyA protein, was identified in *Dictyostelium* (a bacterivore protist naturally found in the soil microflora) and was reported to interact directly with breast carcinoma-amplified sequence 3 protein (BCAS3), and that KinkyA-BCAS3 complex plays an important role in early phagosome formation (22). Another recent study in which BCAS3 and C16orf70 were individually deleted or overexpressed in HeLa and HEK293 cells revealed the presence of BCAS3 and C16orf70 proteins in phagophore assembly site (23). In addition, at

least one clinical study has identified that the unknown gene C16orf70 is altered in some forms of schizophrenia (122).

1.8. Aims of this study

The main aim of this thesis is to evaluate the expression and the functional importance of MYTHO in regulating skeletal muscle mass, structure, and contractile function under basal conditions. We hypothesize that MYTHO is essential for autophagosome formation and determines muscle fibre size and function in healthy skeletal muscles. To achieve these aims, we will use a loss-of-function approach to downregulate MYTHO protein levels in limb muscles of mice by injecting adeno-associated viruses (AAVs) expressing MYTHO short hairpin RNA (shRNA), a powerful technique of RNA interference (RNAi) — also referred as gene silencing. Autophagy, fibre size, and contractile function of limb muscles will be measured 12 weeks after AAV injection.

SECTION 2: MATERIALS AND METHODS

2.1. Animal procedures and AAV injection in skeletal muscle

All experiments were approved by the Research Ethics Board of the Research Institute of the McGill University Health Centre and are in accordance with the principles outlined by the Canadian Council of Animal Care. Adult (approximately 10-week-old) male WT C57/B16j mice (Charles River Laboratories, Saint-Constant, QC) were used for our experiments. All mice were group housed under standard 12:12h light/dark cycle with food and water available *ad libitum*. All AAV used in the present study were purchased from Vector Labs (Burlingame, CA, USA) and were of Serotype I, a serotype with a proven tropism for skeletal muscle cells. After a 7-day acclimatization period, an AAV containing a U6 promoter, a sequence coding for a shRNA targeted the product of the 230025D16Rik gene (the gene coding for MYTHO) was injected intra-muscularly (i.m.) (25µl per site; 1.5×10^{11} gc) into the right tibialis anterior (TA) and gastrocnemius (GAS) muscles. This AAV is hereafter referred as AAV-shRNA-MYTHO. A control AAV containing a scrambled shRNA targeting sequence under the control of the U6 promoter was injected into the contralateral leg. This AAV is hereafter referred as AAV-shRNA-Scrmb. Injections were carried out under general anaesthesia using (2.5 to 3.5%) isoflurane.

2.2. Tissue collection

Twelve weeks after the injection of AAVs, mice were anaesthetized with isoflurane and subsequently sacrificed by cervical dislocation. The TA and GAS from both legs were carefully removed and weighed. The TA were frozen in liquid nitrogen and stored (-80°C) for immunoblotting and quantitative real-time PCR experiments.

2.3. Immunoblotting

Frozen skeletal muscle tissues, approximately 15-30mg were homogenized in an ice-cold lysis buffer (50mM Hepes, 150mM NaCl, 100mM NaF, 5mM EDTA, 0.5% Triton X-100, 0.1 mM DTT, 2 µg/ml leupeptin, 100 µg/ml PMSF, 2 µg/ml aprotinin, and 1 mg/100 ml pepstatin A, pH 7.2) using Mini-beadbeater (BioSpec Products) with ceramic bead at 60Hz. Muscle homogenates were kept on ice for 30 min with periodic agitation and then were centrifuged at 5000 g for 15 min at 4°C, supernatants were collected, and pellets were discarded. The protein content in each sample were determined using the Bradford method. Aliquots of crude muscle homogenate were mixed with Laemmli buffer (6X, reducing buffer, #BP111R, Boston BioProducts) and subsequently denatured for 5 min at 95°C. Equal amounts of protein extracts (20 µg per lanes) were separated by SDS-PAGE, and then transferred onto polyvinylidene difluoride (PVDF) membranes (Bio-Rad Laboratories) using a wet transfer technique. The total proteins on membranes were detected with Ponceau-S solution (Sigma #P3504). Membranes were blocked in PBS + 1% Tween® 20 + 5% bovine serum albumin (BSA) for 1 hour at room temperature and then incubated with the specific primary antibodies (Table 1) overnight at 4°C. Membranes were washed in PBST (3x5 min) and incubated with HRP-conjugated secondary anti-rabbit or anti-mouse secondary antibodies for 1 hour at room temperature, before further washing in PBST (3x5 min). Immunoreactivity were detected using enhanced chemiluminescence substrate (ECL) (Pierce™, Thermo Fisher Scientific) with the ChemiDoc™ Imaging System. The optical densities (OD) of protein bands were quantified using ImageLab software (Bio-Rad Laboratories) and normalized to loading control (Ponceau-stained PVDF membranes or GAPDH). Immunoblotting data are expressed as relative to AAV-shRNA-ScrmB.

2.4. RNA extraction and quantitative real-time PCR

Total RNA was extracted from frozen muscle samples using a PureLink™ RNA Mini Kit (Invitrogen Canada, Burlington, ON). Quantification and purity of RNA was assessed using the A260/A280 absorption method. Total RNA (2 µg) was reverse transcribed using a Superscript II® Reverse Transcriptase Kit and random primers (Invitrogen Canada, Burlington, ON). Reactions were incubated at 42°C for 50min and at 90°C for 5min. Real-time PCR detection of mRNA expression was performed using a Prism® 7000 Sequence Detection System (Applied Biosystems, Foster City, CA). Cycle threshold (CT) values were obtained for each target gene. Δ CT values (normalized gene expression) were calculated as CT of target gene minus CT of the geometric means of three housekeeping genes (*18S*, *β -Actin*, *Cyclophilin* and *Gapdh*). Relative mRNA level quantifications of target genes were determined using the threshold cycle ($\Delta\Delta$ CT) method, as compared to AAV-shRNA-ScrmB. The primer sequences for all genes are found in Table 2.

2.5. Muscle sections for histology analysis

TA samples were mounted in tragacanth (Sigma-Aldrich #G1128) on plastic blocks and frozen in liquid isopentane cooled in liquid nitrogen and stored at -80°C. Samples were cut into 10µm cross-sections using a cryostat at -20°C then mounted on lysine coated slides (Superfrost), as described in (123, 124). Cross-sections were brought to room temperature, rehydrated with PBS (pH 7.2), then blocked with goat serum (10% in PBS). They were then incubated with primary polyclonal anti-laminin rabbit IgG antibody (Sigma-Aldrich #L9393) for 1 h at room temperature. Sections were then washed three times in PBS before being incubated for 1 h at room temperature with an Alexa Fluor® 594 goat anti-rabbit IgG antibody (A-11037, Invitrogen, Waltham, MA). Sections were then washed three times in PBS and slides were cover slipped using ProLong™ Gold Antifade Mountant with DAPI as a mounting

medium. Slides were imaged with a Zeiss fluorescence microscope (Zeiss Axio Imager 2). Median distribution of minimum Feret diameters and centrally located nuclei were analyzed using ImageJ (NIH, Bethesda, MD) (125). Sections were also stained for IgG to examine necrotic myofibres.

2.6. *In situ* determination of fibre typology

TA muscle sections were immunolabeled for MyHC types IIA and IIB, as previously described (123, 126). Cross-sections were brought to room temperature, rehydrated with PBS (pH 7.2), then blocked with goat serum (10% in PBS). They were then incubated for 1 h at room temperature with the following primary antibody cocktail: mouse IgG1 monoclonal anti-MyHC type IIA (SC-71), mouse IgM monoclonal anti-MyHC type IIB (BF-F3, 1:200), and rabbit IgG polyclonal anti-Laminin (Sigma-Aldrich #L9393). Sections were then washed three times in PBS before being incubated for 1 h at room temperature with the following Alexa Fluor® secondary antibody cocktail: Alexa Fluor® 594 goat anti-mouse IgG1 (y1) (A-21125), Alexa Fluor® 488 goat anti-mouse IgM (A-21042,1:500), and Alexa Fluor® 488 goat anti-rabbit IgG (A-11008). They were then washed three times in PBS and slides were cover slipped using Prolong™ Gold (P36930) as a mounting medium. Images were captured using a Zeiss Axio Imager M2. All MyHC-targeting primary antibodies were purchased from the Developmental Studies Hybridoma Bank (DSHB) at the University of Iowa.

2.7. Transmission electron microscopy

Small strips prepared from white GAS fibres were fixed in 2% glutaraldehyde buffer solution in 0.1 M cacodylate, pH 7.4, then post-fixed in 1% osmium tetroxide in 0.1 M cacodylate buffer. Tissues were dehydrated using a gradient of increasing concentrations of methanol to propylene oxide and infiltrated and embedded in EPON™ at the Facility for

Electron Microscopy Research at McGill University. Ultrathin longitudinal sections (60 nm) were cut with a Reichert-Jung Ultracut III ultramicrotome (Leica Microsystems), mounted on nickel carbon-formvar coated grids, and stained with uranyl acetate and lead citrate. Sections were imaged using a FEI Tecnai 12 transmission electron microscope at 120 kV and images were digitally captured using an AMT XR80C CCD camera system.

2.8. *In situ* assessment of muscle contractile function

To determine skeletal muscle contractile function, animals were anesthetized with an intraperitoneal injection of a ketamine-xylazine cocktail (ketamine: 130 mg/kg; xylazine: 20 mg/kg). Anesthesia was maintained with 0.05 ml supplemental doses, as needed. A Dynamic Muscle Control and Analysis Software (DMC/DMA) Suite was used for collection and data analysis (Aurora Scientific, Aurora, ON). The distal tendon of the left TA muscle was isolated and attached to the arm of a 305C-LR dual-mode muscle lever with 4.0 surgical silk, as previously described, with minor modifications (124, 127, 128). The partially exposed muscle surface was kept moist and directly stimulated with an electrode placed on the belly of the muscle. Optimal muscle length and voltage was progressively adjusted to produce maximal tension and length was measured with a microcaliper. The pulse duration was set to 0.2 ms for all tetanic contractions. Force-frequency relationship curves were determined at muscle optimal length at 10, 30, 50, 70, 100, 120, 150 and 200Hz, with 1 min intervals between stimulations to avoid fatigue. At the end of each experiment, mice were sacrificed, and muscles were carefully dissected, weighed, and frozen in liquid nitrogen or in isopentane pre-cooled in liquid nitrogen. *In situ* muscle force was normalized to muscle mass.

2.9. Statistical analyses

All statistical analyses were performed using GraphPad Prism 9.1. When only one variable was compared between AAV-shRNA-Scrb1 and AAV-shRNA-MYH9 injected muscles, differences were tested using paired bilateral student t-tests. When multiple variables were compared, differences between the AAV-shRNA-Scrb1 and AAV-shRNA-MYH9 were analyzed using two-way repeated measures analysis of variance (ANOVA) if there were no missing values or using mixed-effects analysis if there were missing values. Corrections for multiple comparisons following ANOVA or mixed-effects analysis were performed by controlling for the false discovery rate using the two-stage step-up method of Benjamini and Krieger and Yekutieli. p-values <0.05 and q-values <0.1 were considered statistically significant. The exact numbers of animals within each group in all figures are indicated in figure legends. All data in bar graphs are presented as mean \pm SEM.

SECTION 3: RESULTS

3.1. Verification of MYTHO knockdown in limb muscles

To study the functional importance of MYTHO in skeletal muscle under basal condition, we performed i.m. injections of an AAV containing a shRNA targeting D230025D16Rik to knockdown (KD) MYTHO expression in WT C57BL/6J male mice (Figure 1). MYTHO KD was initiated at 10 weeks of age to avoid potential impact on skeletal muscle development. Figure 1 depicts the experimental procedures and protocols. One hindlimb muscles were injected with AAV-shRNA-MYTHO while the contralateral muscles received AAV-shRNA-Scramb. As highlighted in Figure 2&3, muscles that were injected with AAV-shRNA-MYTHO into the TA and GAS resulted in significant decrease in MYTHO mRNA and protein levels relative to contralateral leg injected with AAV-shRNA-Scramb (Figures 2&3).

3.2. Effects of MYTHO knockdown on muscle mass, muscle histology and fibre size

Examination of skeletal muscle mass at 12 weeks post AAV injection revealed significant increase in muscle mass in TA muscles injected with AAV-shRNA-MYTHO (Figure 4). We next assessed histology on skeletal muscle with either AAV-shRNA-Scramb or AAV-shRNA-MYTHO. As shown in figure 5, examination of TA histology 12 weeks post AAV injection revealed significant increase in the number of relatively small fibres containing one or more central nuclei in TA muscles with MYTHO KD (Figure 5). None of these centrally nucleated fibres were detected in the TA muscles injected with AAV-shRNA-Scramb (Figure 5).

Total number of muscle fibres in muscles with MYTHO KD increased significantly relatively to those injected with AAV-shRNA-Scramb however, minimum Feret diameters were not affected by MYTHO KD (Figure 6). These results suggest that despite the increase in the

number of relatively small fibres with central nuclei, total TA fibre size was not different among muscles with MYTHO KD and those injected with AAV-shRNA-Scrm (Figure 7), suggesting that some fibres in TA muscles injected with AAV-shRNA-MYTHO have larger size compared to those with intact MYTHO. This was indeed the case with respect to fibres with minimum Feret diameters between 60 to 75 μm (Figure 7).

To investigate whether MYTHO KD triggered skeletal muscle fibre necrosis, we detected mouse immunoglobulins inside muscle fibres using an anti-mouse secondary antibody (Figure 8). We reasoned those necrotic fibres have leaky cell membranes allowing the entry of plasma into muscle fibres. While no positive fibres were detected in muscles injected with AAV-shRNA-Scrm, several fibres in muscles injected with AAV-shRNA-MYTHO were positive for mouse immunoglobulins suggesting that these fibres are undergoing necrosis (Figure 8).

3.3. Effects of MYTHO knockdown on muscle fibre type

We observe in Figure 9 the effects of MYTHO KD on fibre type distribution in the TA muscle based on the expression of various MyHC isoforms. Muscles injected with AAV-shRNA-MYTHO elicited significant decrease in the proportion of type IIA and a significant increase in the proportion of type IIB but had not influence on the proportion of type IIX fibres and type IIA/IIX hybrid fibres (Figure 9). In addition, MYTHO KD triggered significant decrease in minimum Feret diameters of type IIX fibres and an increase in minimum Feret diameters of type IIB fibres while minimum Feret diameters of type IIA and IIA/IIX fibres were not affected by MYTHO KD (Figure 9).

3.4. Effects of MYTHO knockdown on markers of muscle fibre regeneration

To investigate whether fibre necrosis associated with MYTHO KD is associated with muscle fibre regeneration, we detected mRNA levels of four markers of muscle regeneration (myogenesis): embryonic myosin heavy chain (*Myh3*), neonatal myosin heavy chain (*Myh8*), transcription factor *MyoD* and transcription factor *Myogenin*. Figure 10 indicates that mRNA levels of *Myh8*, but not *Myh3*, increased significantly in TA muscles injected with AAV-shRNA-MYTHO relative to those injected with AAV-shRNA-Scrm. In addition, MYTHO KD fibres elicited significant increase in mRNA levels of *Myogenin*, but not *MyoD* levels (Figure 10).

3.5. Effects of MYTHO knockdown on muscle ultrastructure

Transmission electron microscopy (TEM) images of white GAS muscles injected with AAV-shRNA-Scrm are demonstrated in Figure 11. Normal mitochondrial, SR, and T-tubule morphology were observed. However, in GAS muscles injected with AAV-shRNA-MYTHO, abnormal tubular aggregates and dilated SR were frequently observed (Figure 12 A, B & D). In addition, abnormally shaped intermyofibrillar and subsarcolemmal mitochondria were also detected (Figure 12 B & F). Finally, large accumulation of glycogen (black arrows in C) and lamellar bodies (white arrows in E & F) were also detected in muscles with MYTHO KD.

3.6. Effects of MYTHO knockdown on the autophagy pathway

To assess the effects of MYTHO KD on the autophagy proteolytic pathway, we first measured mRNA expression of various autophagy-related genes in the TA muscles. Then, we evaluated the changes in LC3B protein lipidation using immunoblotting and assessed changes in protein levels of p62/SQSTM1 and BNIP3 (marker of mitophagy). Figure 13 depicts changes in the expression of genes involved in various steps of autophagosome formation. The

expression of two members of the *Beclin1* complex (*Beclin1* and *Vps34*) decreased significantly in response to MYTHO KD. No significant changes in the expression of *Wipi2*, *Sqstm1*, *Gabarapl1*, *Lc3b*, *Bnip3*, and the lysosome *Cathepsin L* were observed in response to MYTHO KD (Figure 13).

Immunoblotting for LC3B protein revealed significant increase in the intensity of LC3B-I (cytosolic) protein, no changes in LC3B-II (lipidated form) protein levels, and a significant decrease in LC3B-II/LC3B-I ratios (index of autophagosome formation) in response to MYTHO KD (Figure 14). Neither BNIP3 protein levels nor those of p62/SQSTM1 protein were affected by MYTHO KD (Figures 14 and 15).

3.7. Effects of MYTHO knockdown on muscle contractility

Measurements of TA *in situ* force-frequency relationship revealed that muscles injected with AAV-shRNA-MYTHO generated significantly lower isometric force at a given stimulation frequency relative to those with intact MYTHO (Figure 16).

SECTION 4: DISCUSSION

The main observations associated with twelve weeks of MYTHO KD in mouse limb muscles are: 1) Increased muscle mass; 2) The presence of a relatively large number of small fibres with centrally located nuclei; 3) The presence of necrotic fibres which contained immunoglobulins; 4) Changes in fibre type distribution manifested as a decrease in proportion of type IIA fibres and an increase in the proportion of type IIB fibres; 5) Induction of markers of muscle regeneration; 6) Significant ultrastructural changes with tubular aggregates, dilated SR, abnormally shaped mitochondria and the presence of lamellar bodies; 7) Decreased basal autophagy as indicated by the decline in LC3B-II/LC3B-I ratios; and finally 8) Significant decrease in skeletal muscle contractility.

To our knowledge, the current study is the first to examine functional significance of MYTHO in skeletal muscles. As previously mentioned, our collaborators, Dr. Sandri's research group, have identified C16orf70 (D230025D16Rik, in mice) as a FoxO-dependent gene which is significantly induced in several models of skeletal muscle atrophy in mice. This identification was achieved by comparing limb muscle transcriptomes of acutely starved WT mice to those of transgenic mice with FoxO^{1,3,4} KO (21). C16orf70 is highly conserved across species, from *C. elegans* to humans with 95% of homology of the amino acid sequence between mice and humans. Studies on *C. elegans* by Sandri's group revealed that knocking down T01G9.2 (the annotated MYTHO ortholog in nematodes) resulted in decreased movement, dramatic reductions in life span and inhibition of autophagy (Sandri, personal communication). As previously described, based on these findings, Sandri's creative group named this gene with the acronym derived from **Macroautophagy** regulator and **Youth Optimizer**. To assess the functional importance of MYTHO in regulating skeletal muscle function, we used loss-of-function approach. In this case, a particularly powerful technique of gene silencing (a type of RNAi) in which AAVs expressing shRNA for MYTHO were injected into limb muscles of

adult mice, while the contralateral muscles were injected with AAVs expressing scrambled shRNA sequence. The main advantage of the experimental design of our study is that each animal is its own control, with muscles from one leg exposed to the experimental treatment (downregulated MYTHO) and the contralateral leg used as a control (normal MYTHO). Figures 2 and 3 indicate that we have successfully decreased MYTHO mRNA and protein levels in the TA and GAS muscles twelve weeks post AAV injection. Importantly, using similar experimental procedures, our groups have previously shown that such intra-muscular injections of serotype 1 AAVs result in the transduction of virtually all TA, GAS and EDL fibres (129-132). In pilot experiments, we observed significant decrease in muscle MYTHO protein levels even three- and six-weeks post injection. These observations suggest that the use of AAVs expressing shRNA for MYTHO is an appropriate loss-of-function approach to evaluate the functional importance of this gene in regulating skeletal muscle function.

To evaluate the functional role of MYTHO protein in regulating autophagy in skeletal muscles, we measured mRNA expression of several autophagy-related genes and monitored protein levels of LC3B, p62/SQSTM1 and BNIP3. We found that *Beclin1* and *Vps34* (both members of the BECLIN1 complex) mRNA levels decreased significantly in limb muscles injected with AAV-shRNA-MYTHO. Moreover, MYTHO KD elicited a significant increase in the cytosolic form of LC3B (LC3B-I), with no changes in the lipidated form (LC3B-II), and a significant decrease in LC3B-II/LC3B-I ratio (index of autophagosome formation) in response to MYTHO KD. BECLIN1 and VPS34 are essential for autophagosome formation and a decrease in LC3B-II/LC3B-I ratio is generally interpreted as decreased incorporation of LC3B protein into autophagosome membrane when autophagy is impaired (99). Our results suggest that MYTHO KD is associated with decreased skeletal muscle autophagy. The mechanisms through which MYTHO regulates autophagy are not clear. We propose two possible mechanisms through which MYTHO regulates autophagy.

First, we speculate that MYTHO interacts with WIPI2, a protein essential for autophagosome formation from phagophores, and with LC3B, a protein involved in autophagosome membrane structure. In addition, we suspect that MYTHO interaction with WIPI2 and LC3B proteins is essential for the elongation step of autophagosome formation (Figure 17). WIPI2 functions as a PI3P effector, bridging PI3P production with recruitment of the ATG16L complex for LC3B (133). MYTHO has been identified in two independent screens as an interactor of WIPI2/ATG18 (134, 135). Our analysis of MYTHO interactome, using the Biophysical Interactions of ORFeome-derived complexes—*BioPlex* network (<https://bioplex.hms.harvard.edu/>) (136), revealed that MYTHO is likely to interact with several proteins, including WIPI2 (Figure 18). Our proposal that MYTHO interacts with LC3B is because MYTHO contains several WD40 domains and putative LIR motifs (Figure 19). WD40 domains provide protein-protein interaction platforms; several autophagy-related proteins contain this domain (137). LIR motifs are essential for protein-LC3 interactions and are present in members of the basal autophagy apparatus and in autophagy cargo receptors (138). Future studies should be dedicated to investigating the direct interactions between MYTHO, WIPI2, and LC3B and the importance of this interaction to autophagosome formation.

Second, during the completion of our experiments, Kojima and colleagues (23) published a study in 2021 indicating that C16orf70 and BCAS3 form a complex, which is essential for phagophore formation during both non-selective and selective autophagy. They used *in silico* structural modelling, mutational analyses in cell cultures and *in vitro* phosphoinositide-binding assays and concluded that WD40 repeat domain of human BCAS3 directly binds PI3P. They also reported that overexpression of BCAS3-C16orf70 complex influences the recruitment of several core autophagy proteins to the phagophore assembly site. These results indicate that BCAS3 and MYTHO play critical roles in autophagosome

formation. Another study that supports important roles for BCAS3 and MYTHO in the regulation of autophagy was published in 2020 by Yamada and Schaap (22) who identified KinkyA and DDB_G0272949, homologs of C16orf70 and BCAS3, respectively, as genes involved in spore formation in *Dictyostelium*, a species of soil-dwelling amoeba. These authors also reported that autophagic activity as evaluated by the efficiency of Atg8 delivery to lysosomes was impaired when either KinkyA or DDB_G0272949 were deleted in *Dictyostelium*. Our analyses of D230025D16Rik and C16orf70 protein interactomes using the Biological General Repository for Interaction Datasets (*BioGRID*) (<https://thebiogrid.org/>) (139) and *GeneMANIA* (<https://genemania.org/>) (140) indicate that MYTHO protein physically interacts with BCAS3 protein (Figures 20 and 21). It should be emphasized that the findings of Kojima et al. were made in cultured cells and those of Yamada and Schapp were in *Dictyostelium*. Whether the interaction between MYTHO and BCAS3 occurs in *in vivo* settings and regulates autophagosome formation in skeletal muscles remain to be investigated. Currently, there is no published studies documenting the presence and functional importance of BCAS3 protein in skeletal muscle fibres.

Another interesting observation in our study is the presence of relatively large number of small diameter fibres containing one or more central nuclei in muscles with MYTHO KD. This observation suggests that downregulation of MYTHO expression compromised muscle fibre integrity and led to fibre necrosis; and that necrosis was followed by activation and differentiation of satellite cells into new muscle fibres. This proposal is based on the well-established sequential events that are triggered by injury and necrosis of mature skeletal muscle fibres. These events include infiltration and phagocytosis of myofibre debris by macrophages, revascularization of injured muscle, activation, and proliferation of muscle precursors (satellite cells), differentiation and fusion of satellite cells, and finally myotube formation and innervation (141, 142). Two more observations support the proposal that fibre necrosis

developed in muscles with MYTHO KD, namely, the presence of few fibres that stained positively for mouse immunoglobulins (leaky cell membrane) indicating these fibres were undergoing necrosis, and the upregulation of *Myh8* which under normal conditions is transiently expressed during fetal development and disappears shortly after birth. However, this MyHC isoform is re-expressed during muscle regeneration and is considered as a specific marker of regenerating fibres in muscle pathologies (142, 143). The mechanisms through which downregulation of MYTHO expression by AAV-shRNA-MYTHO causes fibre necrosis and regeneration remain unclear. We propose three possible explanations.

First, it is possible that inhibition of basal autophagy in fibres with MYTHO KD could have triggered fibre necrosis. Masiero et al. (102) assessed muscle phenotypical changes associated with muscle-selective deletion of *Atg7* in mice and found several spots of myofibre necrosis and degeneration, they suggested that these findings could be associated to inhibition of autophagy. However, these authors also concluded that necrotic fibres in *Atg7* deficient muscles were rare and scattered between normal myofibres (102). We believe that the contribution of autophagy inhibition to the development of fibre necrosis in muscles with MYTHO KD may have been relatively small.

The second possible mechanism behind the development of fibre necrosis in response to MYTHO KD is the development of tubular aggregates which were evident on examination under TEM. Tubular aggregates originating from the SR have been described in aged skeletal muscles and in several neuromuscular disorders such as Duchenne muscular dystrophy, alcohol- and drug-induced myopathies, inherited myasthenia, and in genetic muscle diseases (tubular aggregate myopathies) (144-147). Boncompagni et al. (148) proposed that tubular aggregates are the consequence of swelling of the SR cisternae extending into longitudinally oriented tubules. There is also a consensus that in patients with tubular aggregate myopathies, SR swelling is the result of excessive cytosolic or intraluminal Ca^{2+} levels and that aggregates

contain several proteins involved in storage and update of Ca^{2+} such as SERCA, STIM1, Ryanodine receptor type 1, and Sarcolumenin are localized to tubular aggregates (145, 149, 150). There is also evidence that excessive oligomerization of STIM1 (the main Ca^{2+} sensor in the SR) can trigger the formation of tubular aggregates (149). In addition, cytoskeletal proteins such as Spectrin, Dystrophin, Desmin and heat shock proteins have also been detected in tubular aggregates (150, 151). Tubular aggregates and the formation of lamellar bodies associated with MYTHO KD are similar to those detected in skeletal muscles of mice deficient in Carboxyl Terminus of Hsc70-Interacting Protein (CHIP) (144). Schisler and colleagues proposed that alterations of heat shock proteins that normally interact with CHIP might have contributed to the build-up of toxic oligomers and tubular aggregate in CHIP KD muscles (144). These observations suggest that MYTHO may interact with proteins involved in Ca^{2+} homeostasis, cytoskeletal proteins and heat shock proteins, and that decreased MYTHO protein levels in fibres with MYTHO KD might have disrupted intracellular Ca^{2+} homeostasis and triggered the accumulation of these proteins into SR tubular aggregates. One of these proteins is Ataxin-3 (Atxn3) which is predicted to directly interact with MYTHO (Figures 20 and 21). Ataxin 3 is a deubiquitinating enzyme localized at the endoplasmic reticulum (ER) and is involved in the phenomenon of retrotranslocation of misfolded proteins from the ER to the cytosol where they are eliminated by the proteasome. Retrotranslocation of misfolded proteins requires a complex consisting of p97 ATPase, Ufd1, and Npl4. There is evidence that Ataxin 3 promotes P97-associated deubiquitination and facilitates the transfer of polypeptides from p97 to the proteasome; and that mutation or decreased Ataxin 3 activity leads to accumulation of misfolded proteins in the ER and the development of ER stress (152). Ataxin 3 is also involved in the regulation of Ca^{2+} homeostasis of the ER and mutation or decreased activity of this protein causes major disruption of Ca^{2+} intracellular homeostasis (153). The direct

association of MYTHO with Ataxin 3 in skeletal muscles and the influence of MYTHO KD on Ataxin 3 and deubiquitination activity remain to be investigated in future studies.

Third, it is possible that the development of fibre necrosis in muscles with MYTHO KD is the result of mitochondrial defects. We detected significant number of abnormally shaped intermyofibrillar and subsarcolemmal mitochondria in muscles with MYTHO KD. Indeed, enlarged and abnormally folded mitochondria localized within or near dilated SR and T-tubules structures were detected in the intermyofibrillar regions in response to MYTHO KD (Figure 12). Abnormally shaped mitochondria were also evident in the subsarcolemmal space (Figure 12). The exact cause of these morphological mitochondrial abnormalities and the implication of these morphological defects to overall muscle mitochondrial function including respiration and ROS production remain to be investigated. It is possible that morphological anomalies of mitochondria are primary defects triggered by MYTHO KD or they could be a secondary development due to the formation of tubular aggregates that can compress intermyofibrillar mitochondria. But the findings of major morphological abnormalities detected specifically in subsarcolemmal mitochondria suggests that they may be also a primary response to MYTHO KD.

In addition to the development of tubular aggregates and mitochondrial morphological abnormalities, we detected the presence of lamellar bodies (also known as myeloid bodies, lysosomal lamellar bodies or onionoid bodies) in the GAS muscles with MYTHO KD (Figures 12 & 22). Early observations by Bonilla and colleagues (154) have indicated that lamellar bodies are organelles which consist of concentric lamellae, are present in the periphery of skeletal muscles, and are largely composed of phospholipids and proteins (154). In a subsequent study, Reasor (155) concluded that lamellar bodies are dysfunctional lysosomes that fail to degrade phospholipids due to inhibition of lysosomal phospholipase A and C; and that several cationic amphiphilic drugs such as chloroquine, that inhibit lysosomal function,

elicit the formation of lysosomal bodies. Under normal physiological conditions, the main function of the lamellar bodies, particularly in lung and bronchial epithelial cells, is to supply specialized lipid components such as dipalmitoylphosphatidylcholine (DPPC) one of the main components of pulmonary surfactant. However, relatively large number of lamellar bodies have been detected in various cells in pathologies such as atherosclerosis, and degenerated nerve fibres and neurons (156). It has also been reported that oxidative stress elicited by inhibition of glutathione synthesis triggers the formation of lamellar bodies and disruption of mitochondrial function in lung cells (157). In skeletal muscles, lamellar body formation is associated with the muscle atrophy and oxidative stress elicited by inhibition of glutathione synthesis (158). In cultured muscle cells, lamellar body formation is significantly induced by deprivation of the amino acid leucine which also elicits severe oxidative stress (159). These observations suggest that the presence of lamellar bodies in GAS muscles with MYTHO KD might be an indicator of the development of oxidative stress. Future studies should be allocated to documenting the indices of oxidative stress such as ROS levels, protein oxidation, products of lipid peroxidation as well as the levels of antioxidant enzymes and non-enzymatic antioxidants such as glutathione.

Another interesting observation in our study is the effect of MYTHO KD on skeletal muscle contractility. We measured *in situ* TA muscle contractility by stimulating the muscle at different frequencies and monitoring the generated isometric tension. Despite the increase in overall muscle weight, TA specific isometric tension at a given stimulation frequency was significantly lower in muscles injected with AAV-shRNA-MYTHO (Figure 16), indicating that MYTHO KD leads to decreased muscle contractility. This observation could be attributed to several factors.

First, loss of mature fibres due to necrosis, followed by regeneration, is expected to be associated with a decrease in specific force generation simply because regenerated fibres are

relatively small in diameter, express neonatal MyHC isoform, and generate less specific tension relative to fully mature muscle fibres. Second, development of tubular aggregates in muscles with MYTHO KD is likely to disrupt normal SR functions including the release of Ca^{2+} from the SR in response to excitation waves delivered through the T-tubules (excitation-contraction coupling) which leads to decreased muscle contractility, particularly in response to low stimulation frequency. Third, mitochondrial morphological defects associated with MYTHO KD are likely to impair normal mitochondrial respiration and proper supply of ATP required for interaction of myosin and actin. Decreased ATP production thereby impairs normal energy supply needed for proper myofibrillar protein interactions.

In summary, the present study provided novel information regarding the functional importance of MYTHO protein in the regulation of skeletal muscle structure and function. I conclude that MYTHO plays important roles in the integrity of skeletal muscle fibres as evidenced by the development of fibre necrosis and the significant decrease in contractility in response to MYTHO KD in murine limb muscles. We also found MYTHO KD causing mitochondrial abnormalities and accumulation of tubular aggregates and lamellar bodies. Finally, we propose that MYTHO plays an important role in the regulation of basal autophagy in skeletal muscle fibres.

SECTION 5: REFERENCES

1. Scott W, Stevens J, Binder-Macleod SA. Human skeletal muscle fiber type classifications. *Phys Ther.* 2001;81(11):1810-6.
2. Muscaritoli M, Anker SD, Argiles J, Aversa Z, Bauer JM, Biolo G, et al. Consensus definition of sarcopenia, cachexia and pre-cachexia: joint document elaborated by Special Interest Groups (SIG) "cachexia-anorexia in chronic wasting diseases" and "nutrition in geriatrics". *Clin Nutr.* 2010;29(2):154-9.
3. Argiles JM, Muscaritoli M. The Three Faces of Sarcopenia. *J Am Med Dir Assoc.* 2016;17(6):471-2.
4. Bauer J, Morley JE, Schols A, Ferrucci L, Cruz-Jentoft AJ, Dent E, et al. Sarcopenia: A Time for Action. An SCWD Position Paper. *J Cachexia Sarcopenia Muscle.* 2019;10(5):956-61.
5. Cruz-Jentoft AJ, Bahat G, Bauer J, Boirie Y, Bruyere O, Cederholm T, et al. Sarcopenia: revised European consensus on definition and diagnosis. *Age Ageing.* 2019;48(1):16-31.
6. Ding S, Dai Q, Huang H, Xu Y, Zhong C. An Overview of Muscle Atrophy. *Adv Exp Med Biol.* 2018;1088:3-19.
7. Epidemiologic and methodologic problems in determining nutritional status of older persons. Proceedings of a conference. Albuquerque, New Mexico, October 19-21, 1988. *Am J Clin Nutr.* 1989;50(5 Suppl):1121-235.
8. Shafiee G, Keshtkar A, Soltani A, Ahadi Z, Larijani B, Heshmat R. Prevalence of sarcopenia in the world: a systematic review and meta- analysis of general population studies. *J Diabetes Metab Disord.* 2017;16:21.
9. Janssen I, Shepard DS, Katzmarzyk PT, Roubenoff R. The healthcare costs of sarcopenia in the United States. *J Am Geriatr Soc.* 2004;52(1):80-5.
10. Bruyere O, Beaudart C, Ethgen O, Reginster JY, Locquet M. The health economics burden of sarcopenia: a systematic review. *Maturitas.* 2019;119:61-9.
11. Bulow J, Ulijaszek SJ, Holm L. Rejuvenation of the term sarcopenia. *J Appl Physiol* (1985). 2019;126(1):255-6.
12. Arora P, Vasa P, Brenner D, Iglar K, McFarlane P, Morrison H, et al. Prevalence estimates of chronic kidney disease in Canada: results of a nationally representative survey. *CMAJ.* 2013;185(9):E417-23.
13. Workeneh BT, Mitch WE. Review of muscle wasting associated with chronic kidney disease. *Am J Clin Nutr.* 2010;91(4):1128S-32S.
14. Suzuki T, Palus S, Springer J. Skeletal muscle wasting in chronic heart failure. *ESC Heart Fail.* 2018;5(6):1099-107.

15. Lad H, Saumur TM, Herridge MS, Dos Santos CC, Mathur S, Batt J, et al. Intensive Care Unit-Acquired Weakness: Not just Another Muscle Atrophying Condition. *Int J Mol Sci.* 2020;21(21).
16. Postigo-Martin P, Cantarero-Villanueva I, Lista-Paz A, Castro-Martin E, Arroyo-Morales M, Seco-Calvo J. A COVID-19 Rehabilitation Prospective Surveillance Model for Use by Physiotherapists. *J Clin Med.* 2021;10(8).
17. Ali AM, Kunugi H. Skeletal Muscle Damage in COVID-19: A Call for Action. *Medicina (Kaunas).* 2021;57(4).
18. Mizushima N, Komatsu M. Autophagy: renovation of cells and tissues. *Cell.* 2011;147(4):728-41.
19. Mizushima N, Levine B, Cuervo AM, Klionsky DJ. Autophagy fights disease through cellular self-digestion. *Nature.* 2008;451(7182):1069-75.
20. Bonaldo P, Sandri M. Cellular and molecular mechanisms of muscle atrophy. *Dis Model Mech.* 2013;6(1):25-39.
21. Milan G, Romanello V, Pescatore F, Armani A, Paik JH, Frasson L, et al. Regulation of autophagy and the ubiquitin-proteasome system by the FoxO transcriptional network during muscle atrophy. *Nat Commun.* 2015;6:6670.
22. Yamada Y, Schaap P. The proppin Bcas3 and its interactor KinkyA localize to the early phagophore and regulate autophagy. *Autophagy.* 2021;17(3):640-55.
23. Kojima W, Yamano K, Kosako H, Imai K, Kikuchi R, Tanaka K, et al. Mammalian BCAS3 and C16orf70 associate with the phagophore assembly site in response to selective and non-selective autophagy. *Autophagy.* 2021:1-26.
24. Schiaffino S, Reggiani C. Fiber types in mammalian skeletal muscles. *Physiol Rev.* 2011;91(4):1447-531.
25. Schiaffino S, Reggiani C, Murgia M. Fiber type diversity in skeletal muscle explored by mass spectrometry-based single fiber proteomics. *Histol Histopathol.* 2020;35(3):239-46.
26. Blaauw B, Schiaffino S, Reggiani C. Mechanisms modulating skeletal muscle phenotype. *Compr Physiol.* 2013;3(4):1645-87.
27. Russell AP. Molecular regulation of skeletal muscle mass. *Clin Exp Pharmacol Physiol.* 2010;37(3):378-84.
28. Bodine SC, Stitt TN, Gonzalez M, Kline WO, Stover GL, Bauerlein R, et al. Akt/mTOR pathway is a crucial regulator of skeletal muscle hypertrophy and can prevent muscle atrophy in vivo. *Nat Cell Biol.* 2001;3(11):1014-9.
29. Stitt TN, Drujan D, Clarke BA, Panaro F, Timofeyeva Y, Kline WO, et al. The IGF-1/PI3K/Akt pathway prevents expression of muscle atrophy-induced ubiquitin ligases by inhibiting FOXO transcription factors. *Mol Cell.* 2004;14(3):395-403.

30. Rhoads RE. Signal transduction pathways that regulate eukaryotic protein synthesis. *J Biol Chem.* 1999;274(43):30337-40.
31. Leger B, Cartoni R, Praz M, Lamon S, Deriaz O, Crettenand A, et al. Akt signalling through GSK-3 β , mTOR and Foxo1 is involved in human skeletal muscle hypertrophy and atrophy. *J Physiol.* 2006;576(Pt 3):923-33.
32. Dobson M, Ramakrishnan G, Ma S, Kaplun L, Balan V, Fridman R, et al. Bimodal regulation of FoxO3 by AKT and 14-3-3. *Biochim Biophys Acta.* 2011;1813(8):1453-64.
33. Phillips SM. Physiologic and molecular bases of muscle hypertrophy and atrophy: impact of resistance exercise on human skeletal muscle (protein and exercise dose effects). *Appl Physiol Nutr Metab.* 2009;34(3):403-10.
34. Hasselgren PO, Menconi MJ, Fared MU, Yang H, Wei W, Evenson A. Novel aspects on the regulation of muscle wasting in sepsis. *Int J Biochem Cell Biol.* 2005;37(10):2156-68.
35. Wing SS, Lecker SH, Jagoe RT. Proteolysis in illness-associated skeletal muscle atrophy: from pathways to networks. *Crit Rev Clin Lab Sci.* 2011;48(2):49-70.
36. Lecker SH, Goldberg AL, Mitch WE. Protein degradation by the ubiquitin-proteasome pathway in normal and disease states. *J Am Soc Nephrol.* 2006;17(7):1807-19.
37. Cohen S, Nathan JA, Goldberg AL. Muscle wasting in disease: molecular mechanisms and promising therapies. *Nat Rev Drug Discov.* 2015;14(1):58-74.
38. Sandri M, Sandri C, Gilbert A, Skurk C, Calabria E, Picard A, et al. Foxo transcription factors induce the atrophy-related ubiquitin ligase atrogin-1 and cause skeletal muscle atrophy. *Cell.* 2004;117(3):399-412.
39. Mammucari C, Milan G, Romanello V, Masiero E, Rudolf R, Del Piccolo P, et al. FoxO3 controls autophagy in skeletal muscle in vivo. *Cell Metab.* 2007;6(6):458-71.
40. Sandri M. Autophagy in skeletal muscle. *FEBS Lett.* 2010;584(7):1411-6.
41. Sorimachi H, Ishiura S, Suzuki K. Structure and physiological function of calpains. *Biochem J.* 1997;328 (Pt 3):721-32.
42. Thornberry NA, Lazebnik Y. Caspases: enemies within. *Science.* 1998;281(5381):1312-6.
43. Goll DE, Thompson VF, Li H, Wei W, Cong J. The calpain system. *Physiol Rev.* 2003;83(3):731-801.
44. Bartoli M, Richard I. Calpains in muscle wasting. *Int J Biochem Cell Biol.* 2005;37(10):2115-33.
45. Vanderklish PW, Bahr BA. The pathogenic activation of calpain: a marker and mediator of cellular toxicity and disease states. *Int J Exp Pathol.* 2000;81(5):323-39.

46. Wei W, Fareed MU, Evenson A, Menconi MJ, Yang H, Petkova V, et al. Sepsis stimulates calpain activity in skeletal muscle by decreasing calpastatin activity but does not activate caspase-3. *Am J Physiol Regul Integr Comp Physiol*. 2005;288(3):R580-90.
47. Supinski GS, Callahan LA. Calpain activation contributes to endotoxin-induced diaphragmatic dysfunction. *Am J Respir Cell Mol Biol*. 2010;42(1):80-7.
48. Tidball JG, Spencer MJ. Expression of a calpastatin transgene slows muscle wasting and obviates changes in myosin isoform expression during murine muscle disuse. *J Physiol*. 2002;545(3):819-28.
49. Jones SW, Hill RJ, Krasney PA, O'Conner B, Peirce N, Greenhaff PL. Disuse atrophy and exercise rehabilitation in humans profoundly affects the expression of genes associated with the regulation of skeletal muscle mass. *FASEB J*. 2004;18(9):1025-7.
50. Hyatt HW, Powers SK. The Role of Calpains in Skeletal Muscle Remodeling with Exercise and Inactivity-induced Atrophy. *Int J Sports Med*. 2020;41(14):994-1008.
51. Du J, Wang X, Miereles C, Bailey JL, Debigare R, Zheng B, et al. Activation of caspase-3 is an initial step triggering accelerated muscle proteolysis in catabolic conditions. *J Clin Invest*. 2004;113(1):115-23.
52. Gao Y, Ordas R, Klein JD, Price SR. Regulation of caspase-3 activity by insulin in skeletal muscle cells involves both PI3-kinase and MEK-1/2. *J Appl Physiol (1985)*. 2008;105(6):1772-8.
53. Belizario JE, Lorite MJ, Tisdale MJ. Cleavage of caspases-1, -3, -6, -8 and -9 substrates by proteases in skeletal muscles from mice undergoing cancer cachexia. *Br J Cancer*. 2001;84(8):1135-40.
54. Whidden MA, Smuder AJ, Wu M, Hudson MB, Nelson WB, Powers SK. Oxidative stress is required for mechanical ventilation-induced protease activation in the diaphragm. *J Appl Physiol (1985)*. 2010;108(5):1376-82.
55. Sandri M, El Meslemani AH, Sandri C, Schjerling P, Vissing K, Andersen JL, et al. Caspase 3 expression correlates with skeletal muscle apoptosis in Duchenne and facioscapulo human muscular dystrophy. A potential target for pharmacological treatment? *J Neuropathol Exp Neurol*. 2001;60(3):302-12.
56. Plant PJ, Bain JR, Correa JE, Woo M, Batt J. Absence of caspase-3 protects against denervation-induced skeletal muscle atrophy. *J Appl Physiol (1985)*. 2009;107(1):224-34.
57. Bell RA, Al-Khalaf M, Megeney LA. The beneficial role of proteolysis in skeletal muscle growth and stress adaptation. *Skelet Muscle*. 2016;6:16.
58. Mitch WE, Goldberg AL. Mechanisms of muscle wasting. The role of the ubiquitin-proteasome pathway. *N Engl J Med*. 1996;335(25):1897-905.

59. Lecker SH, Solomon V, Mitch WE, Goldberg AL. Muscle protein breakdown and the critical role of the ubiquitin-proteasome pathway in normal and disease states. *J Nutr.* 1999;129(1S Suppl):227S-37S.
60. Ciechanover A. The ubiquitin-proteasome pathway: on protein death and cell life. *EMBO J.* 1998;17(24):7151-60.
61. Chau V, Tobias JW, Bachmair A, Marriott D, Ecker DJ, Gonda DK, et al. A multiubiquitin chain is confined to specific lysine in a targeted short-lived protein. *Science.* 1989;243(4898):1576-83.
62. Thrower JS, Hoffman L, Rechsteiner M, Pickart CM. Recognition of the polyubiquitin proteolytic signal. *EMBO J.* 2000;19(1):94-102.
63. Lam YA, Lawson TG, Velayutham M, Zweier JL, Pickart CM. A proteasomal ATPase subunit recognizes the polyubiquitin degradation signal. *Nature.* 2002;416(6882):763-7.
64. Husnjak K, Dikic I. Ubiquitin-binding proteins: decoders of ubiquitin-mediated cellular functions. *Annu Rev Biochem.* 2012;81:291-322.
65. Saeki Y. Ubiquitin recognition by the proteasome. *J Biochem.* 2017;161(2):113-24.
66. Bodine SC, Latres E, Baumhueter S, Lai VK, Nunez L, Clarke BA, et al. Identification of ubiquitin ligases required for skeletal muscle atrophy. *Science.* 2001;294(5547):1704-8.
67. Gomes MD, Lecker SH, Jagoe RT, Navon A, Goldberg AL. Atrogin-1, a muscle-specific F-box protein highly expressed during muscle atrophy. *Proc Natl Acad Sci U S A.* 2001;98(25):14440-5.
68. Lagirand-Cantaloube J, Offner N, Csibi A, Leibovitch MP, Batonnet-Pichon S, Tintignac LA, et al. The initiation factor eIF3-f is a major target for atrogin1/MAFbx function in skeletal muscle atrophy. *EMBO J.* 2008;27(8):1266-76.
69. Lagirand-Cantaloube J, Cornille K, Csibi A, Batonnet-Pichon S, Leibovitch MP, Leibovitch SA. Inhibition of atrogin-1/MAFbx mediated MyoD proteolysis prevents skeletal muscle atrophy in vivo. *PLoS One.* 2009;4(3):e4973.
70. Centner T, Yano J, Kimura E, McElhinny AS, Pelin K, Witt CC, et al. Identification of muscle specific ring finger proteins as potential regulators of the titin kinase domain. *J Mol Biol.* 2001;306(4):717-26.
71. Clarke BA, Drujan D, Willis MS, Murphy LO, Corpina RA, Burova E, et al. The E3 Ligase MuRF1 degrades myosin heavy chain protein in dexamethasone-treated skeletal muscle. *Cell Metab.* 2007;6(5):376-85.
72. Cohen S, Brault JJ, Gygi SP, Glass DJ, Valenzuela DM, Gartner C, et al. During muscle atrophy, thick, but not thin, filament components are degraded by MuRF1-dependent ubiquitylation. *J Cell Biol.* 2009;185(6):1083-95.

73. Li YP, Chen Y, Li AS, Reid MB. Hydrogen peroxide stimulates ubiquitin-conjugating activity and expression of genes for specific E2 and E3 proteins in skeletal muscle myotubes. *Am J Physiol Cell Physiol*. 2003;285(4):C806-12.
74. Caron MA, Theriault ME, Pare ME, Maltais F, Debigare R. Hypoxia alters contractile protein homeostasis in L6 myotubes. *FEBS Lett*. 2009;583(9):1528-34.
75. Li YP, Reid MB. NF-kappaB mediates the protein loss induced by TNF-alpha in differentiated skeletal muscle myotubes. *Am J Physiol Regul Integr Comp Physiol*. 2000;279(4):R1165-70.
76. Cai D, Frantz JD, Tawa NE, Jr., Melendez PA, Oh BC, Lidov HG, et al. IKKbeta/NF-kappaB activation causes severe muscle wasting in mice. *Cell*. 2004;119(2):285-98.
77. Wirawan E, Vanden Berghe T, Lippens S, Agostinis P, Vandenabeele P. Autophagy: for better or for worse. *Cell Res*. 2012;22(1):43-61.
78. Sandri M. New findings of lysosomal proteolysis in skeletal muscle. *Curr Opin Clin Nutr Metab Care*. 2011;14(3):223-9.
79. Kon M, Cuervo AM. Chaperone-mediated autophagy in health and disease. *FEBS Lett*. 2010;584(7):1399-404.
80. Orenstein SJ, Cuervo AM. Chaperone-mediated autophagy: molecular mechanisms and physiological relevance. *Semin Cell Dev Biol*. 2010;21(7):719-26.
81. Kaushik S, Cuervo AM. Chaperone-mediated autophagy. *Methods Mol Biol*. 2008;445:227-44.
82. Ravikumar B, Sarkar S, Davies JE, Futter M, Garcia-Arencibia M, Green-Thompson ZW, et al. Regulation of mammalian autophagy in physiology and pathophysiology. *Physiol Rev*. 2010;90(4):1383-435.
83. Choi AM, Ryter SW, Levine B. Autophagy in human health and disease. *N Engl J Med*. 2013;368(7):651-62.
84. Klionsky DJ. Autophagy: from phenomenology to molecular understanding in less than a decade. *Nat Rev Mol Cell Biol*. 2007;8(11):931-7.
85. Kim J, Kundu M, Viollet B, Guan KL. AMPK and mTOR regulate autophagy through direct phosphorylation of Ulk1. *Nat Cell Biol*. 2011;13(2):132-41.
86. Dunlop EA, Hunt DK, Acosta-Jaquez HA, Fingar DC, Tee AR. ULK1 inhibits mTORC1 signaling, promotes multisite Raptor phosphorylation and hinders substrate binding. *Autophagy*. 2011;7(7):737-47.
87. Yu L, McPhee CK, Zheng L, Mardones GA, Rong Y, Peng J, et al. Termination of autophagy and reformation of lysosomes regulated by mTOR. *Nature*. 2010;465(7300):942-6.

88. Hardie DG, Ross FA, Hawley SA. AMPK: a nutrient and energy sensor that maintains energy homeostasis. *Nat Rev Mol Cell Biol.* 2012;13(4):251-62.
89. Hosokawa N, Hara T, Kaizuka T, Kishi C, Takamura A, Miura Y, et al. Nutrient-dependent mTORC1 association with the ULK1-Atg13-FIP200 complex required for autophagy. *Mol Biol Cell.* 2009;20(7):1981-91.
90. Alers S, Löffler AS, Wesselborg S, Stork B. Role of AMPK-mTOR-Ulk1/2 in the regulation of autophagy: cross talk, shortcuts, and feedbacks. *Mol Cell Biol.* 2012;32(1):2-11.
91. Tooze SA, Yoshimori T. The origin of the autophagosomal membrane. *Nat Cell Biol.* 2010;12(9):831-5.
92. He C, Levine B. The Beclin 1 interactome. *Curr Opin Cell Biol.* 2010;22(2):140-9.
93. Sun Q, Fan W, Zhong Q. Regulation of Beclin 1 in autophagy. *Autophagy.* 2009;5(5):713-6.
94. Tanida I. Autophagosome formation and molecular mechanism of autophagy. *Antioxid Redox Signal.* 2011;14(11):2201-14.
95. Mizushima N, Kuma A, Kobayashi Y, Yamamoto A, Matsubae M, Takao T, et al. Mouse Apg16L, a novel WD-repeat protein, targets to the autophagic isolation membrane with the Apg12-Apg5 conjugate. *J Cell Sci.* 2003;116(Pt 9):1679-88.
96. Kabeya Y, Mizushima N, Ueno T, Yamamoto A, Kirisako T, Noda T, et al. LC3, a mammalian homologue of yeast Apg8p, is localized in autophagosome membranes after processing. *EMBO J.* 2000;19(21):5720-8.
97. Fullgrabe J, Klionsky DJ, Joseph B. The return of the nucleus: transcriptional and epigenetic control of autophagy. *Nat Rev Mol Cell Biol.* 2014;15(1):65-74.
98. Tanida I, Minematsu-Ikeguchi N, Ueno T, Kominami E. Lysosomal turnover, but not a cellular level, of endogenous LC3 is a marker for autophagy. *Autophagy.* 2005;1(2):84-91.
99. Klionsky DJ, Abeliovich H, Agostinis P, Agrawal DK, Aliev G, Askew DS, et al. Guidelines for the use and interpretation of assays for monitoring autophagy in higher eukaryotes. *Autophagy.* 2008;4(2):151-75.
100. Kimura S, Noda T, Yoshimori T. Dynein-dependent movement of autophagosomes mediates efficient encounters with lysosomes. *Cell Struct Funct.* 2008;33(1):109-22.
101. Yang Z, Huang J, Geng J, Nair U, Klionsky DJ. Atg22 recycles amino acids to link the degradative and recycling functions of autophagy. *Mol Biol Cell.* 2006;17(12):5094-104.
102. Masiero E, Agatea L, Mammucari C, Blaauw B, Loro E, Komatsu M, et al. Autophagy is required to maintain muscle mass. *Cell Metab.* 2009;10(6):507-15.

103. Adhihetty PJ, O'Leary MF, Chabi B, Wicks KL, Hood DA. Effect of denervation on mitochondrially mediated apoptosis in skeletal muscle. *J Appl Physiol* (1985). 2007;102(3):1143-51.
104. O'Leary MF, Vainshtein A, Carter HN, Zhang Y, Hood DA. Denervation-induced mitochondrial dysfunction and autophagy in skeletal muscle of apoptosis-deficient animals. *Am J Physiol Cell Physiol*. 2012;303(4):C447-54.
105. O'Leary MF, Hood DA. Denervation-induced oxidative stress and autophagy signaling in muscle. *Autophagy*. 2009;5(2):230-1.
106. Youle RJ, Narendra DP. Mechanisms of mitophagy. *Nat Rev Mol Cell Biol*. 2011;12(1):9-14.
107. Callahan LA, Supinski GS. Sepsis-induced myopathy. *Crit Care Med*. 2009;37(10 Suppl):S354-67.
108. Callahan LA, Stofan DA, Szweda LI, Nethery DE, Supinski GS. Free radicals alter maximal diaphragmatic mitochondrial oxygen consumption in endotoxin-induced sepsis. *Free Radic Biol Med*. 2001;30(1):129-38.
109. Boveris A, Alvarez S, Navarro A. The role of mitochondrial nitric oxide synthase in inflammation and septic shock. *Free Radic Biol Med*. 2002;33(9):1186-93.
110. Callahan LA, Supinski GS. Sepsis induces diaphragm electron transport chain dysfunction and protein depletion. *Am J Respir Crit Care Med*. 2005;172(7):861-8.
111. Brealey D, Brand M, Hargreaves I, Heales S, Land J, Smolenski R, et al. Association between mitochondrial dysfunction and severity and outcome of septic shock. *Lancet*. 2002;360(9328):219-23.
112. Brealey D, Karyampudi S, Jacques TS, Novelli M, Stidwill R, Taylor V, et al. Mitochondrial dysfunction in a long-term rodent model of sepsis and organ failure. *Am J Physiol Regul Integr Comp Physiol*. 2004;286(3):R491-7.
113. Mofarrahi M, Sigala I, Guo Y, Godin R, Davis EC, Petrof B, et al. Autophagy and skeletal muscles in sepsis. *PLoS One*. 2012;7(10):e47265.
114. Mizushima N, Yamamoto A, Matsui M, Yoshimori T, Ohsumi Y. In vivo analysis of autophagy in response to nutrient starvation using transgenic mice expressing a fluorescent autophagosome marker. *Mol Biol Cell*. 2004;15(3):1101-11.
115. Hanai J, Cao P, Tanksale P, Imamura S, Koshimizu E, Zhao J, et al. The muscle-specific ubiquitin ligase atrogin-1/MAFbx mediates statin-induced muscle toxicity. *J Clin Invest*. 2007;117(12):3940-51.
116. Sandri M, Lin J, Handschin C, Yang W, Arany ZP, Lecker SH, et al. PGC-1alpha protects skeletal muscle from atrophy by suppressing FoxO3 action and atrophy-specific gene transcription. *Proc Natl Acad Sci U S A*. 2006;103(44):16260-5.

117. Moylan JS, Smith JD, Chambers MA, McLoughlin TJ, Reid MB. TNF induction of atrogen-1/MAFbx mRNA depends on Foxo4 expression but not AKT-Foxo1/3 signaling. *Am J Physiol Cell Physiol.* 2008;295(4):C986-93.
118. Hussain SN, Mofarrahi M, Sigala I, Kim HC, Vassilakopoulos T, Maltais F, et al. Mechanical ventilation-induced diaphragm disuse in humans triggers autophagy. *Am J Respir Crit Care Med.* 2010;182(11):1377-86.
119. Kamei Y, Miura S, Suzuki M, Kai Y, Mizukami J, Taniguchi T, et al. Skeletal muscle FOXO1 (FKHR) transgenic mice have less skeletal muscle mass, down-regulated Type I (slow twitch/red muscle) fiber genes, and impaired glycemic control. *J Biol Chem.* 2004;279(39):41114-23.
120. Zhao J, Brault JJ, Schild A, Cao P, Sandri M, Schiaffino S, et al. FoxO3 coordinately activates protein degradation by the autophagic/lysosomal and proteasomal pathways in atrophying muscle cells. *Cell Metab.* 2007;6(6):472-83.
121. Howe KL, Achuthan P, Allen J, Allen J, Alvarez-Jarreta J, Amode MR, et al. *Ensembl* 2021. *Nucleic Acids Res.* 2021;49(D1):D884-D91.
122. Rukova B, Staneva R, Hadjidekova S, Stamenov G, Milanova V, Toncheva D. Whole genome methylation analyses of schizophrenia patients before and after treatment. *Biotechnol Biotechnol Equip.* 2014;28(3):518-24.
123. Leduc-Gaudet JP, Picard M, St-Jean Pelletier F, Sgarioto N, Auger MJ, Vallee J, et al. Mitochondrial morphology is altered in atrophied skeletal muscle of aged mice. *Oncotarget.* 2015;6(20):17923-37.
124. Leduc-Gaudet J-P, Reynaud O, Hussain SN, Gouspillou G. Parkin overexpression protects from ageing-related loss of muscle mass and strength. *The Journal of Physiology.* 2019;0(0).
125. Briguet A, Courdier-Fruh I, Foster M, Meier T, Magyar JP. Histological parameters for the quantitative assessment of muscular dystrophy in the mdx-mouse. *Neuromuscul Disord.* 2004;14(10):675-82.
126. Leduc-Gaudet J-P, Miguez K, Cefis M, Moamer A, Chaffer TJ, Faitg J, et al. Role of autophagy in sepsis-induced skeletal muscle dysfunction, whole-body metabolism, and survival. *bioRxiv.* 2021:2021.08.05.455081.
127. Mofarrahi M, McClung JM, Kontos CD, Davis EC, Tappuni B, Moroz N, et al. Angiotensin-1 enhances skeletal muscle regeneration in mice. *Am J Physiol Regul Integr Comp Physiol.* 2015;308(7):R576-89.
128. Gouspillou G, Godin R, Piquereau J, Picard M, Mofarrahi M, Mathew J, et al. Protective role of Parkin in skeletal muscle contractile and mitochondrial function. *The Journal of physiology.* 2018;596(13):2565-79.
129. Dulac M, Leduc-Gaudet JP, Cefis M, Ayoub MB, Reynaud O, Shams A, et al. Regulation of muscle and mitochondrial health by the mitochondrial fission protein Drp1 in aged mice. *J Physiol.* 2021.

130. Dulac M, Leduc-Gaudet JP, Reynaud O, Ayoub MB, Guerin A, Finkelchtein M, et al. Drp1 knockdown induces severe muscle atrophy and remodelling, mitochondrial dysfunction, autophagy impairment and denervation. *J Physiol*. 2020;598(17):3691-710.
131. Leduc-Gaudet JP, Reynaud O, Hussain SN, Gouspillou G. Parkin overexpression protects from ageing-related loss of muscle mass and strength. *J Physiol*. 2019;597(7):1975-91.
132. Leduc-Gaudet JP, Mayaki D, Reynaud O, Broering FE, Chaffer TJ, Hussain SNA, et al. Parkin Overexpression Attenuates Sepsis-Induced Muscle Wasting. *Cells*. 2020;9(6).
133. Dooley HC, Razi M, Polson HE, Girardin SE, Wilson MI, Tooze SA. WIPI2 links LC3 conjugation with PI3P, autophagosome formation, and pathogen clearance by recruiting Atg12-5-16L1. *Mol Cell*. 2014;55(2):238-52.
134. Huttlin EL, Bruckner RJ, Paulo JA, Cannon JR, Ting L, Baltier K, et al. Architecture of the human interactome defines protein communities and disease networks. *Nature*. 2017;545(7655):505-9.
135. Bakula D, Muller AJ, Zuleger T, Takacs Z, Franz-Wachtel M, Thost AK, et al. WIPI3 and WIPI4 beta-propellers are scaffolds for LKB1-AMPK-TSC signalling circuits in the control of autophagy. *Nat Commun*. 2017;8:15637.
136. Huttlin EL, Ting L, Bruckner RJ, Gebreab F, Gygi MP, Szpyt J, et al. The BioPlex Network: A Systematic Exploration of the Human Interactome. *Cell*. 2015;162(2):425-40.
137. Xu C, Min J. Structure and function of WD40 domain proteins. *Protein Cell*. 2011;2(3):202-14.
138. Birgisdottir AB, Lamark T, Johansen T. The LIR motif - crucial for selective autophagy. *J Cell Sci*. 2013;126(Pt 15):3237-47.
139. Oughtred R, Rust J, Chang C, Breitkreutz BJ, Stark C, Willems A, et al. The BioGRID database: A comprehensive biomedical resource of curated protein, genetic, and chemical interactions. *Protein Sci*. 2021;30(1):187-200.
140. Franz M, Rodriguez H, Lopes C, Zuberi K, Montojo J, Bader GD, et al. GeneMANIA update 2018. *Nucleic Acids Res*. 2018;46(W1):W60-W4.
141. Ciciliot S, Schiaffino S. Regeneration of mammalian skeletal muscle. Basic mechanisms and clinical implications. *Curr Pharm Des*. 2010;16(8):906-14.
142. Schiaffino S, Rossi AC, Smerdu V, Leinwand LA, Reggiani C. Developmental myosins: expression patterns and functional significance. *Skelet Muscle*. 2015;5:22.
143. Winter A, Bornemann A. NCAM, vimentin and neonatal myosin heavy chain expression in human muscle diseases. *Neuropathol Appl Neurobiol*. 1999;25(5):417-24.

144. Schisler JC, Patterson C, Willis MS. Skeletal Muscle Mitochondrial Alterations in Carboxyl Terminus of Hsc70 Interacting Protein (Chip) *-/-* Mice. *Afr J Cell Pathol.* 2016;6(4):28-36.
145. Chevessier F, Bauche-Godard S, Leroy JP, Koenig J, Paturneau-Jouas M, Eymard B, et al. The origin of tubular aggregates in human myopathies. *J Pathol.* 2005;207(3):313-23.
146. Engel WK, Bishop DW, Cunningham GG. Tubular aggregates in type II muscle fibers: ultrastructural and histochemical correlation. *J Ultrastruct Res.* 1970;31(5-6):507-25.
147. Muller HD, Vielhaber S, Brunn A, Schroder JM. Dominantly inherited myopathy with novel tubular aggregates containing 1-21 tubulofilamentous structures. *Acta Neuropathol.* 2001;102(1):27-35.
148. Boncompagni S, Protasi F, Franzini-Armstrong C. Sequential stages in the age-dependent gradual formation and accumulation of tubular aggregates in fast twitch muscle fibers: SERCA and calsequestrin involvement. *Age (Dordr).* 2012;34(1):27-41.
149. Bohm J, Chevessier F, Maues De Paula A, Koch C, Attarian S, Feger C, et al. Constitutive activation of the calcium sensor STIM1 causes tubular-aggregate myopathy. *Am J Hum Genet.* 2013;92(2):271-8.
150. Chevessier F, Marty I, Paturneau-Jouas M, Hantai D, Verdier-Sahuque M. Tubular aggregates are from whole sarcoplasmic reticulum origin: alterations in calcium binding protein expression in mouse skeletal muscle during aging. *Neuromuscul Disord.* 2004;14(3):208-16.
151. Manta P, Terzis G, Papadimitriou C, Kontou C, Vassilopoulos D. Emerin expression in tubular aggregates. *Acta Neuropathol.* 2004;107(6):546-52.
152. Wang Q, Li L, Ye Y. Regulation of retrotranslocation by p97-associated deubiquitinating enzyme ataxin-3. *J Cell Biol.* 2006;174(7):963-71.
153. Chen X, Tang TS, Tu H, Nelson O, Pook M, Hammer R, et al. Deranged calcium signaling and neurodegeneration in spinocerebellar ataxia type 3. *J Neurosci.* 2008;28(48):12713-24.
154. Bonilla E, Schotland DL, Wakayama Y. Lamellar bodies at the cell periphery of human muscle fibers. *Eur J Cell Biol.* 1979;20(2):159-67.
155. Reasor MJ. A review of the biology and toxicologic implications of the induction of lysosomal lamellar bodies by drugs. *Toxicol Appl Pharmacol.* 1989;97(1):47-56.
156. Schmitz G, Muller G. Structure and function of lamellar bodies, lipid-protein complexes involved in storage and secretion of cellular lipids. *J Lipid Res.* 1991;32(10):1539-70.
157. Martensson J, Jain A, Frayer W, Meister A. Glutathione metabolism in the lung: inhibition of its synthesis leads to lamellar body and mitochondrial defects. *Proc Natl Acad Sci U S A.* 1989;86(14):5296-300.

158. Liaghati A, Pileggi CA, Parmar G, Patten DA, Hadzimustafic N, Cuillerier A, et al. Grx2 Regulates Skeletal Muscle Mitochondrial Structure and Autophagy. *Front Physiol.* 2021;12:604210.
159. Rahman M, Mofarrahi M, Kristof AS, Nkengfac B, Harel S, Hussain SN. Reactive oxygen species regulation of autophagy in skeletal muscles. *Antioxid Redox Signal.* 2014;20(3):443-59.

SECTION 6: TABLES

Table 1: Antibodies used for immunoblotting experiments to detect protein expression of various genes in the TA muscles.

Antibody	Source	Catalog	Dilution	Analysis
Rabbit anti-C16orf70 (MYTHO)	Abcam	181.987	1:1000	WB
Rabbit anti-LC3	Cell Signaling	12.741	1:1000	WB
Rabbit anti-p62/SQSTM1	Novus Biologicals Inc.	Clone 2C11	1:1000	WB
Mouse anti-BNIP3	Sigma-Aldrich	B-7931	1:1000	WB
Rabbit anti-GAPDH	Cell signaling	2.118	1:2500	WB
Goat anti-rabbit IgG	Abcam	Ab 6.721	1:5000	WB
Goat anti-mouse IgG	Abcam	Ab 6.728	1:5000	WB

Table 2: Primers used for quantitative real-time PCR experiments to detect mRNA expression of various genes in the TA muscles.

Gene	Forward primer (5'-3')	Reverse primer (3'-5')
<i>D230025D16Rik (Mytho)</i>	CGCTCCTACCATTGAGCAAA	CCTCGGAAGTTGAGGTGGAA
<i>Lc3b</i>	CGATACAAGGGGGAGAAGCA	ACTTCGGAGATGGGAGTGGA
<i>p62/Sqstm1</i>	GCACCTGTCTGAGGGCTTCT	GCTCCAGTTTCCTGGTGGAC
<i>Bnip3</i>	TTCCACTAGCACCTTCTGATGA	GAACACCGCATTTACAGAACAA
<i>Gabarapl1</i>	GAGGACCACCCCTTCG	CGGAGGGCACAAGGTA
<i>Wipi2</i>	TTGATGCAAGTGGGACCAAG	GGAGCAGATGCTCACACACC
<i>Cathepsin L</i>	CGGGTTGCCTAGAAGGACAG	ACAGCCCTGATTGCCTTGAT
<i>18S</i>	TGCGGTTTAGCGTCGGTGTC	CCAAGTGGCCAAAGCGTA
<i>β-Actin</i>	AACCGTGAAAAGATGACCCAG	CACAGCCTGGATGGCTACGTA
<i>Cyclophilin</i>	GCGTCTCTTCGAGCTGTTT	CTGGCACATGAATCCTGGAA
<i>Gapdh</i>	AAGAAGGTGGTGAAGCAGGCG	ACCAGGAAATGAGCTTGACAA

SECTION 7: FIGURES

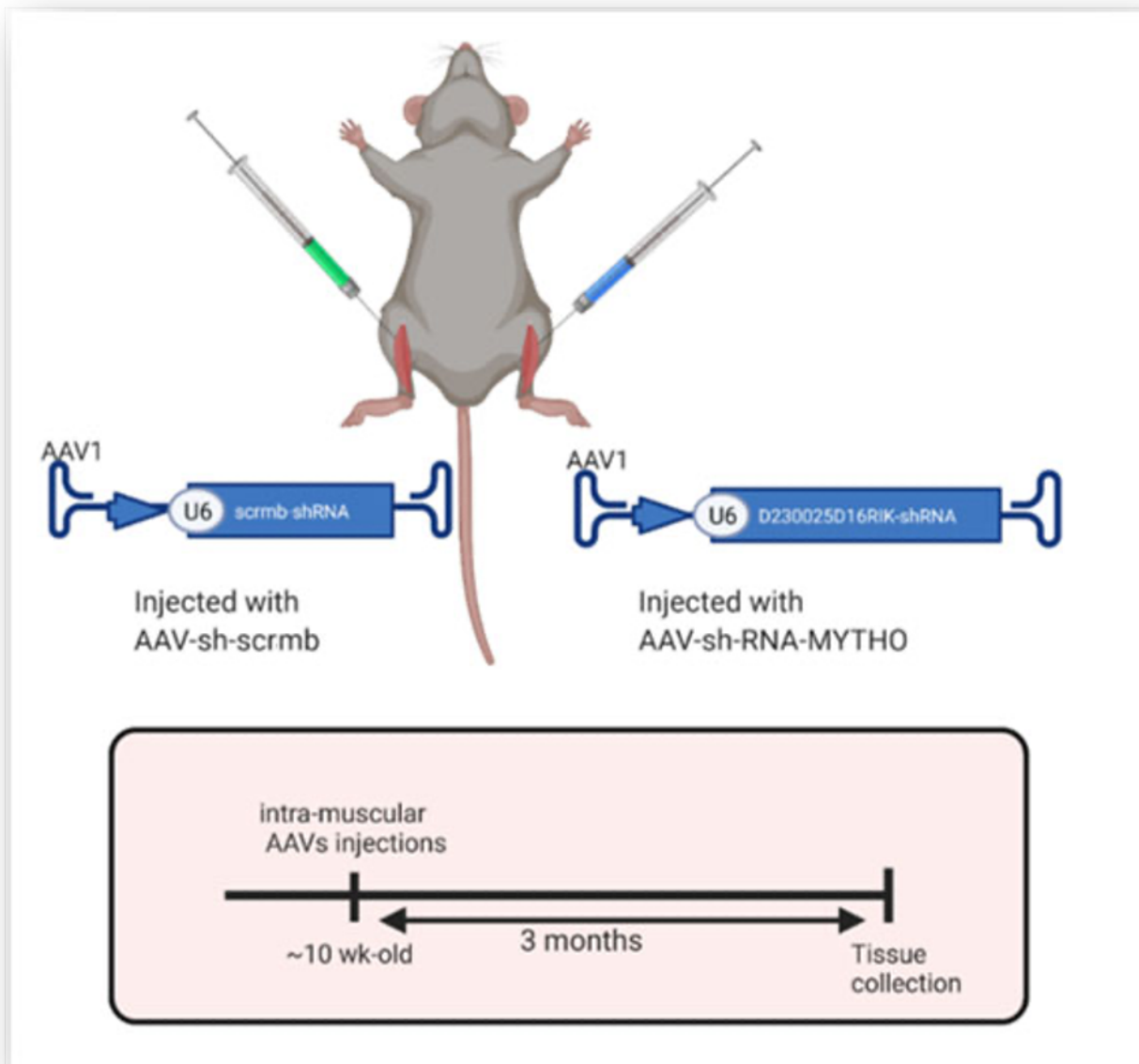


FIGURE 1

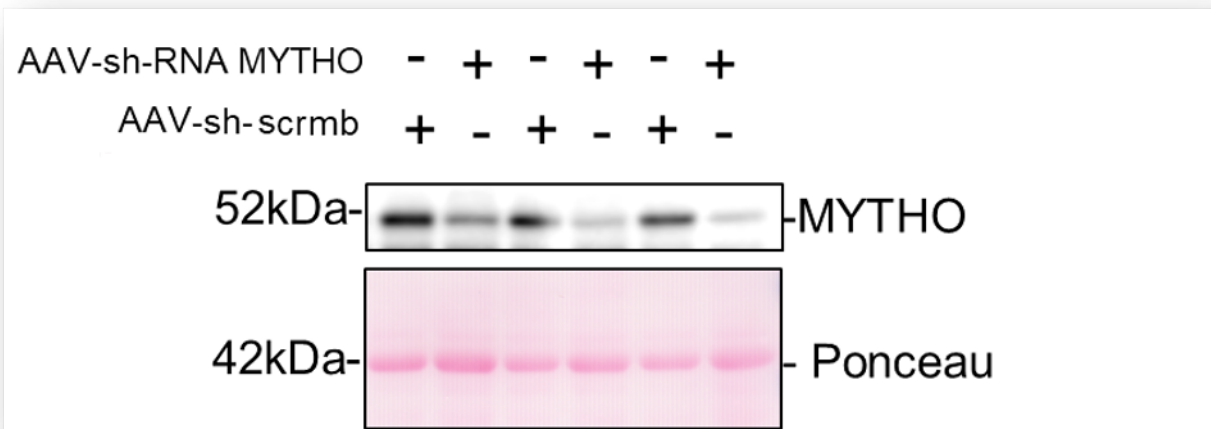


FIGURE 2

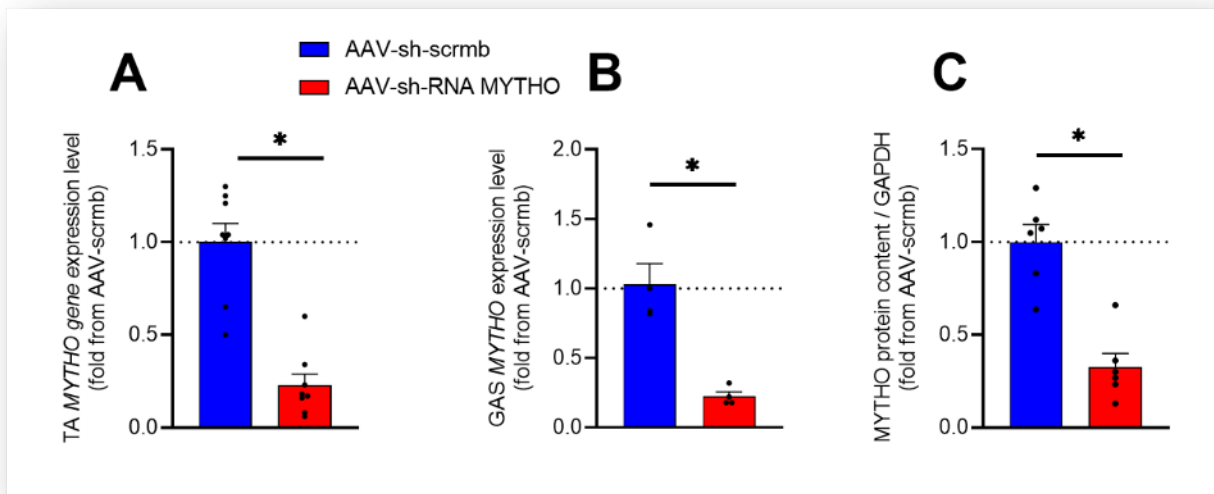


FIGURE 3

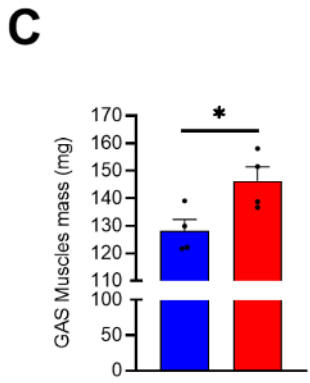
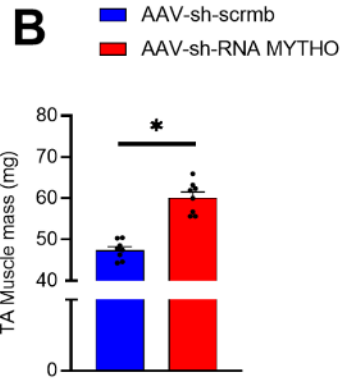
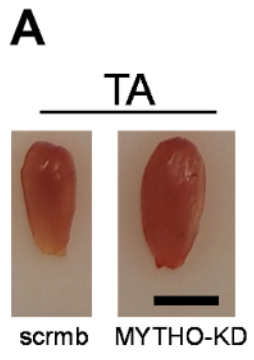


FIGURE 4

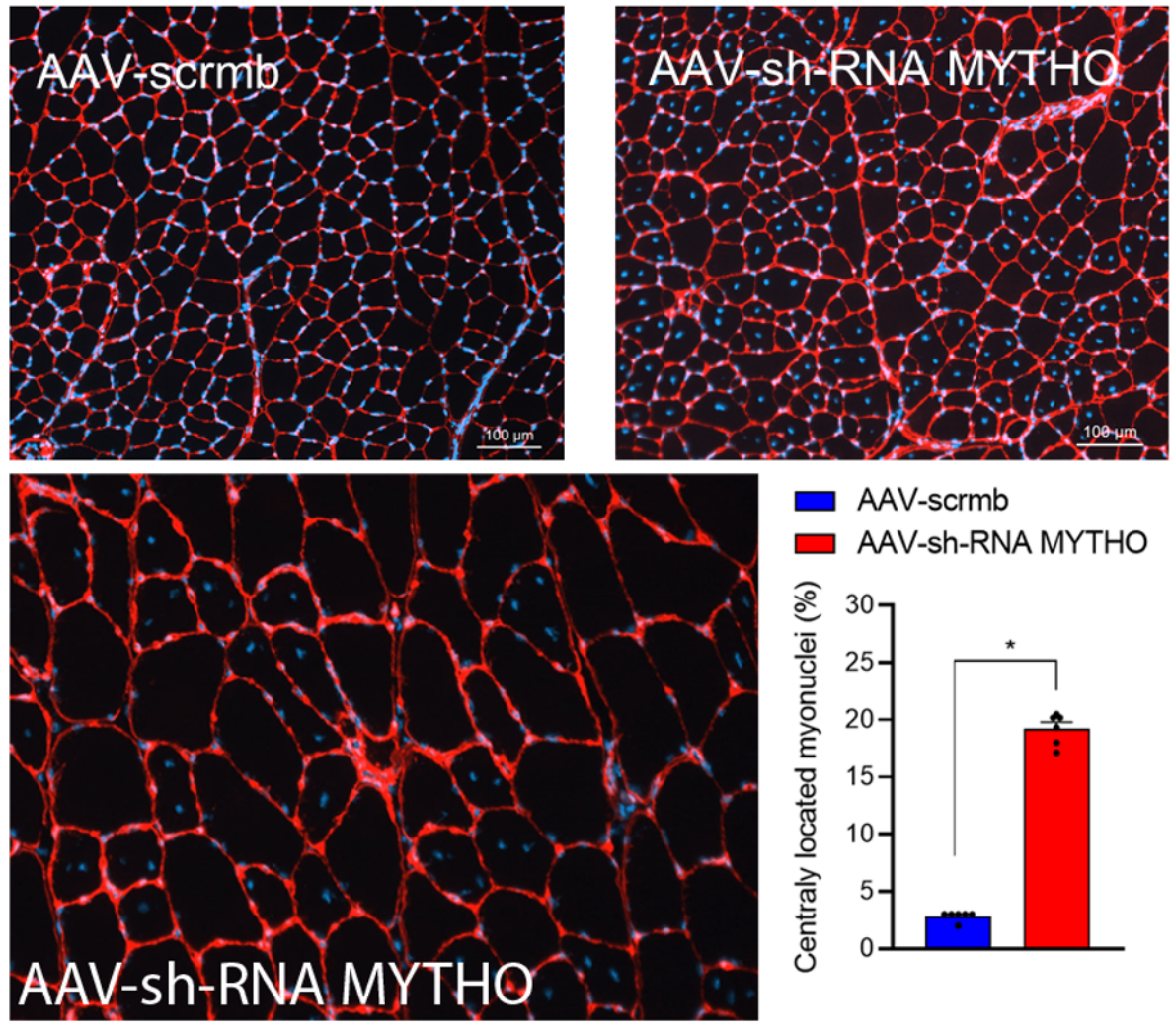


FIGURE 5

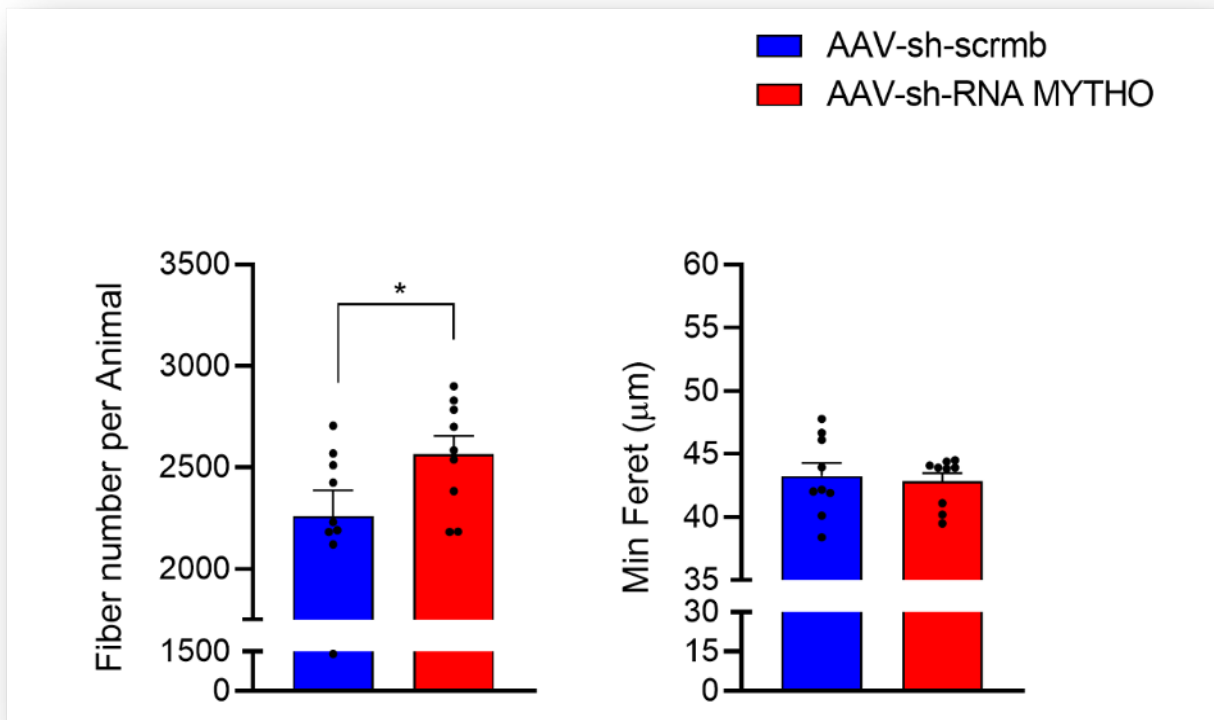


FIGURE 6

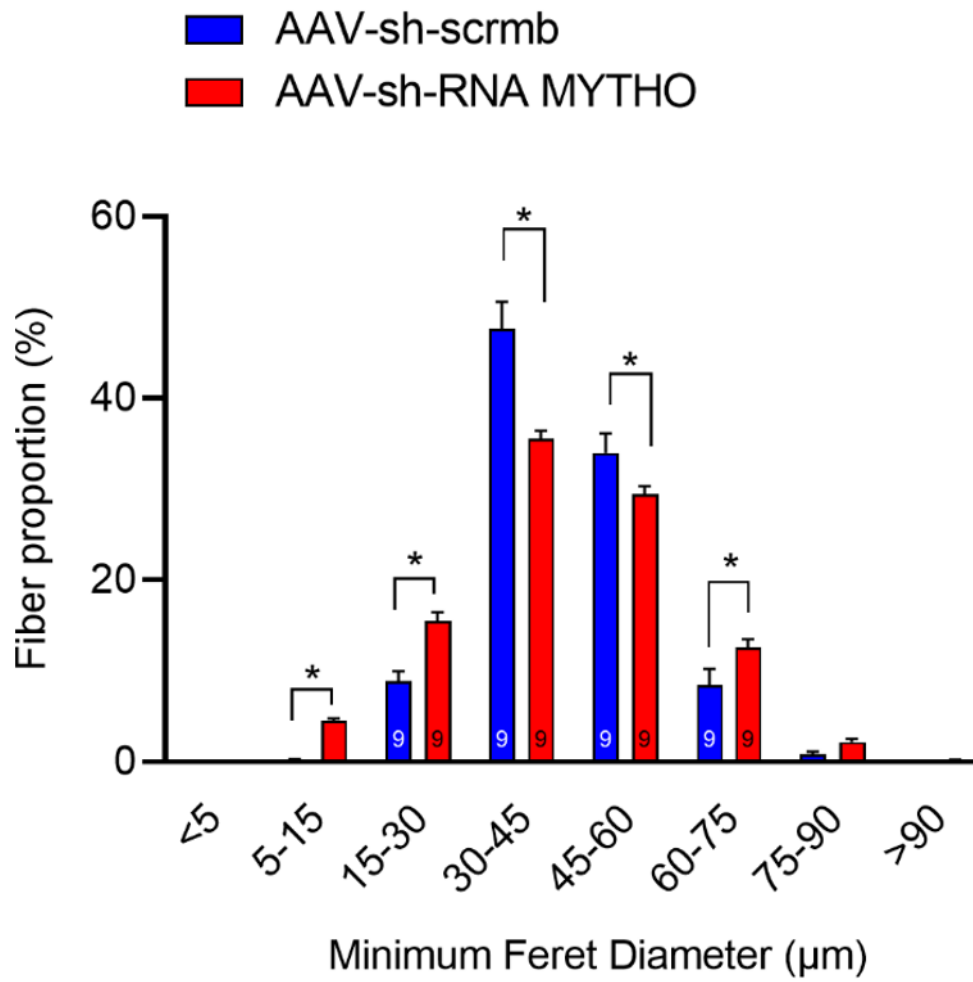


FIGURE 7

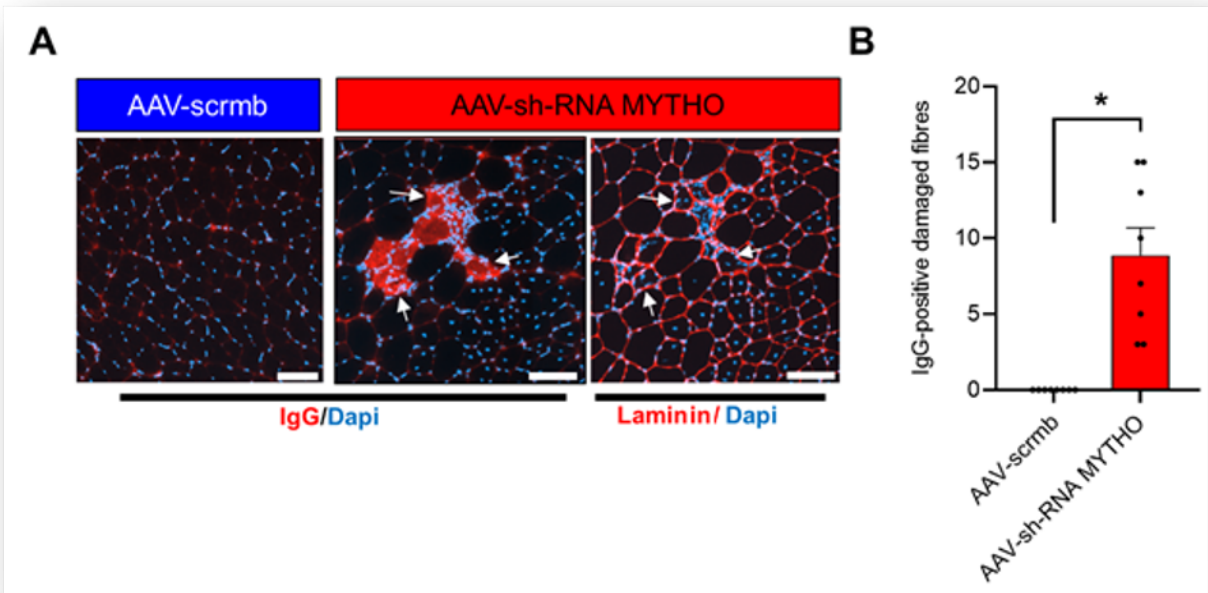


FIGURE 8

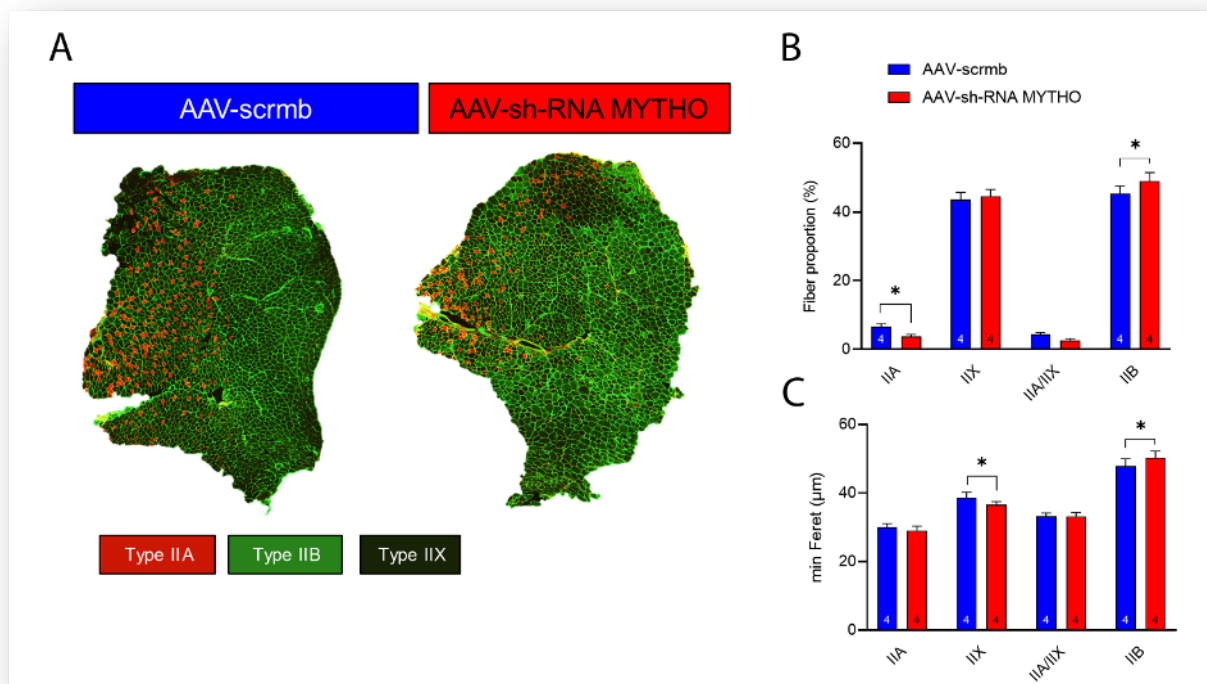


FIGURE 9

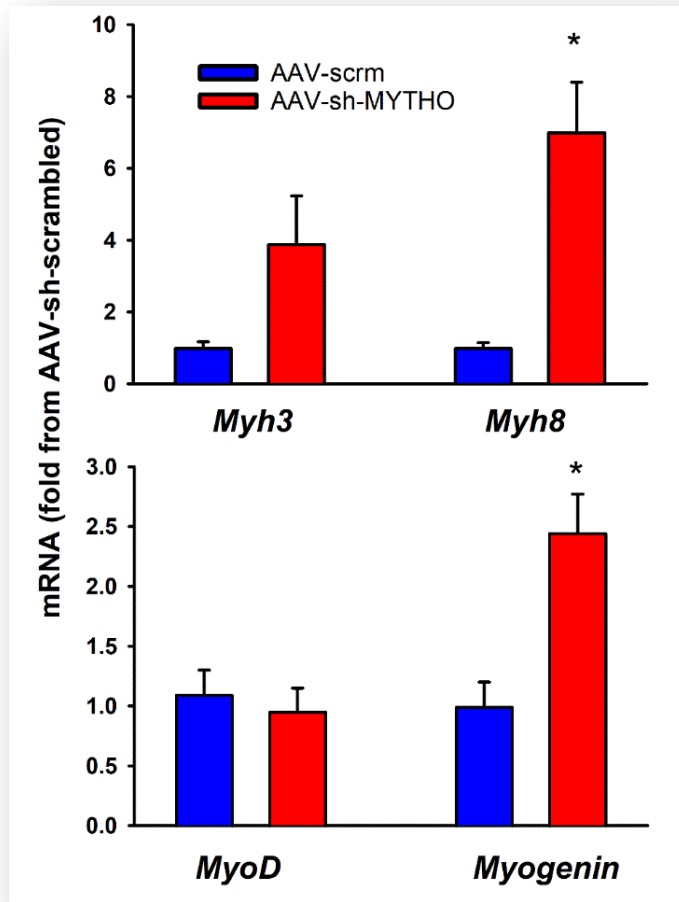


FIGURE 10

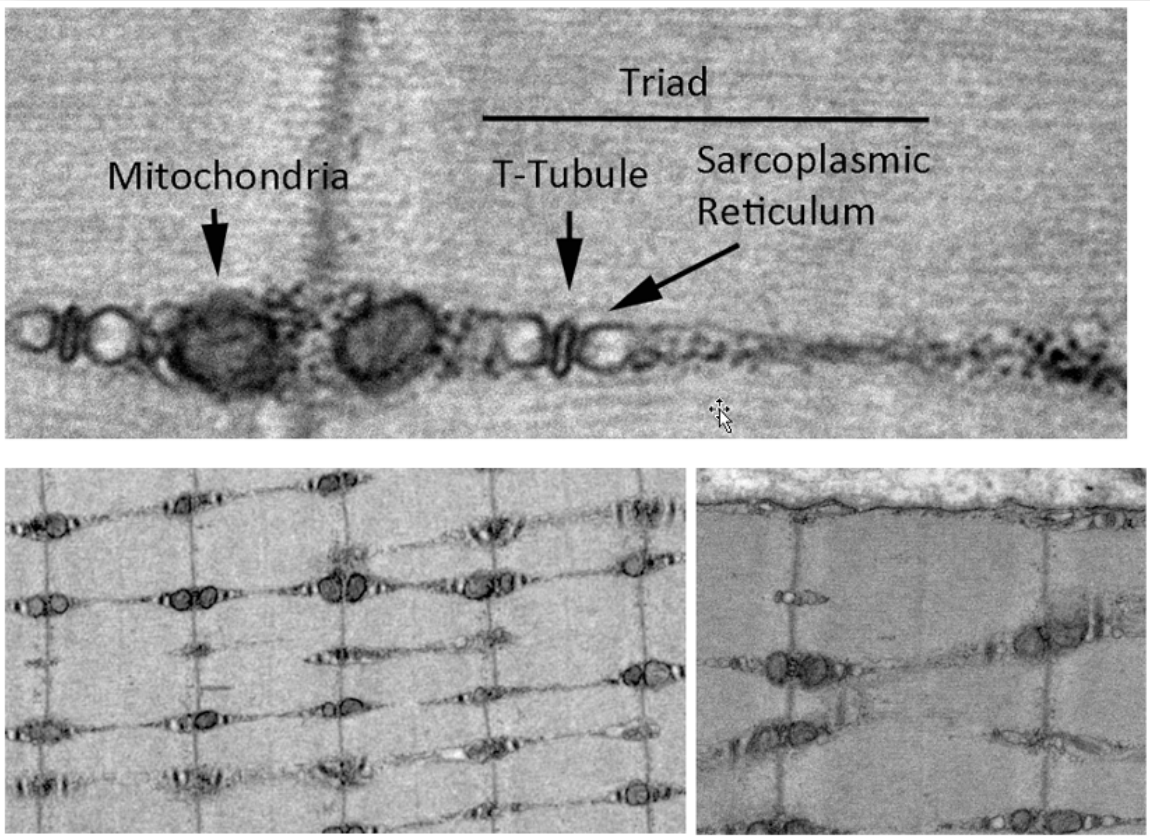


FIGURE 11

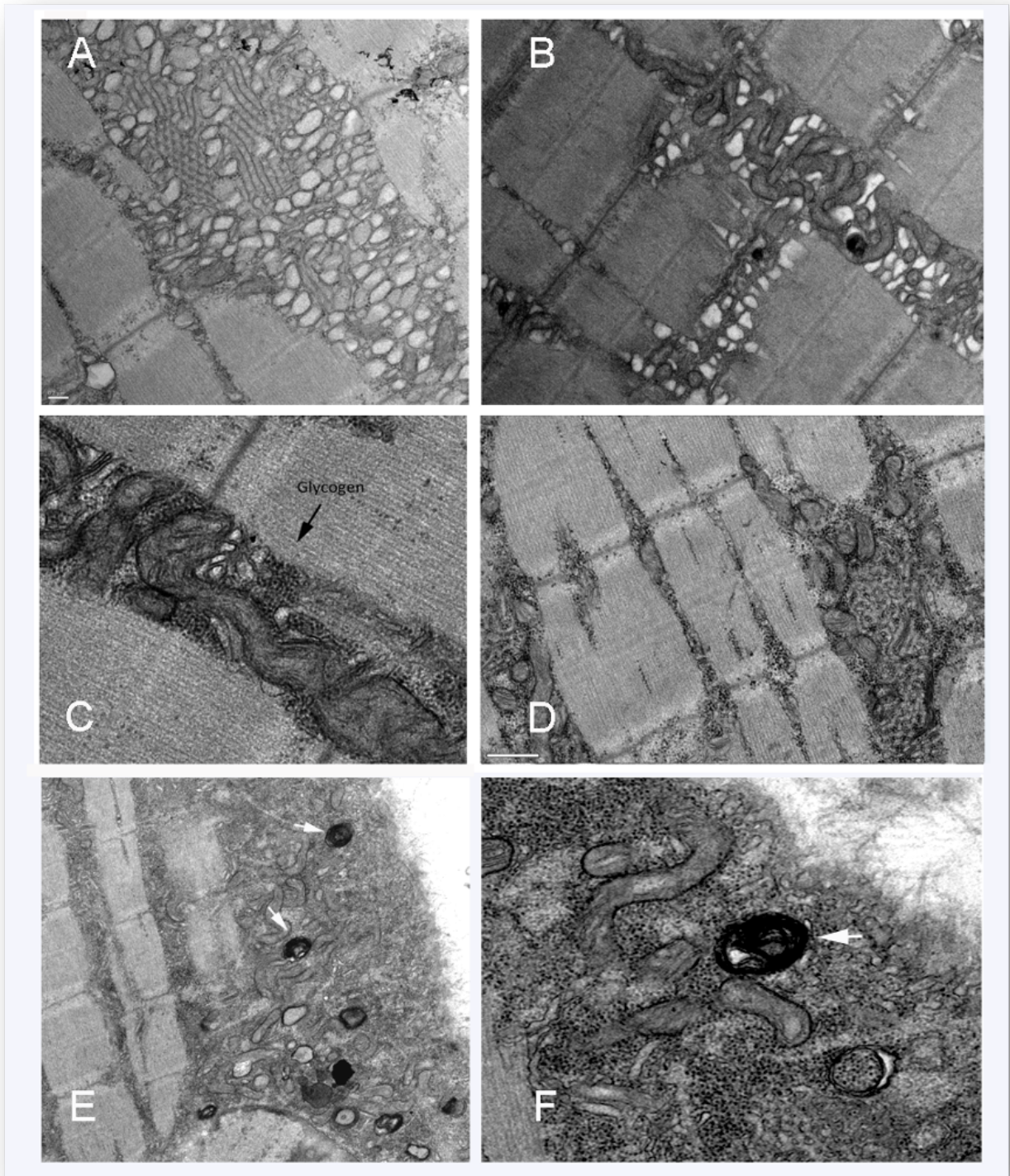


FIGURE 12

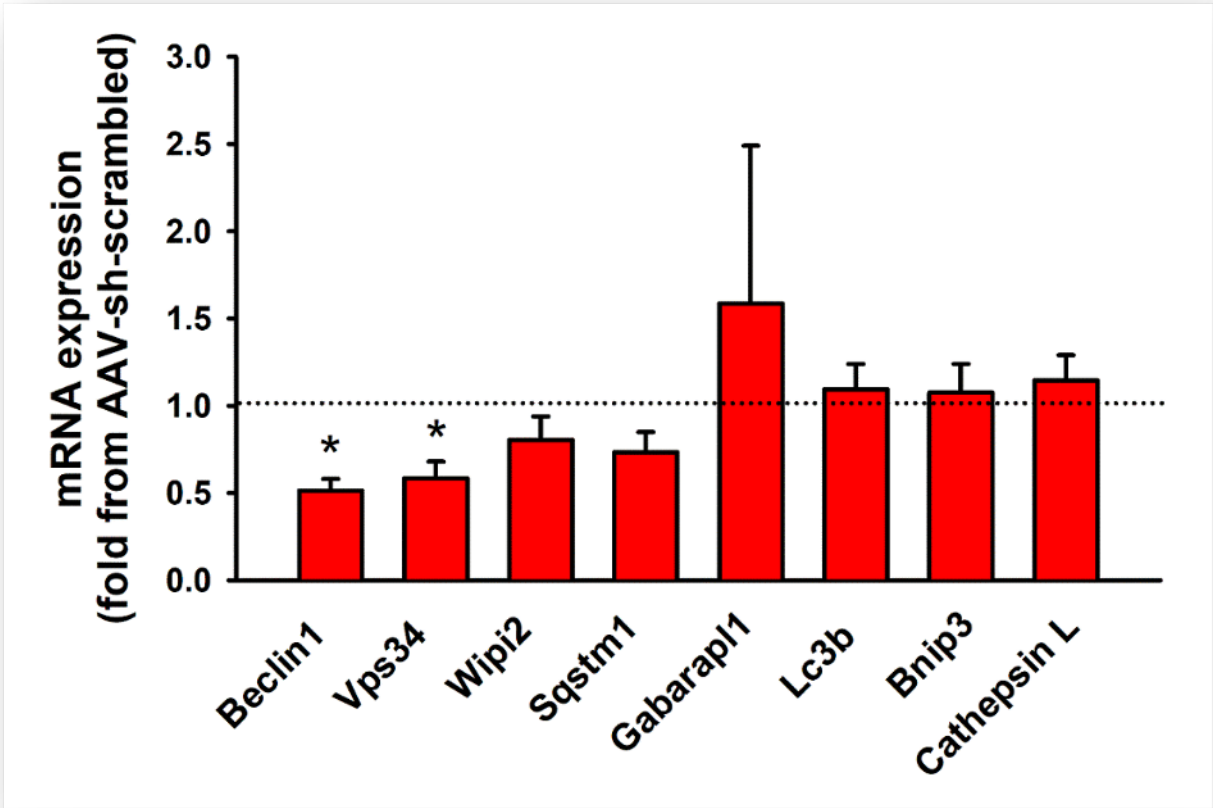


FIGURE 13

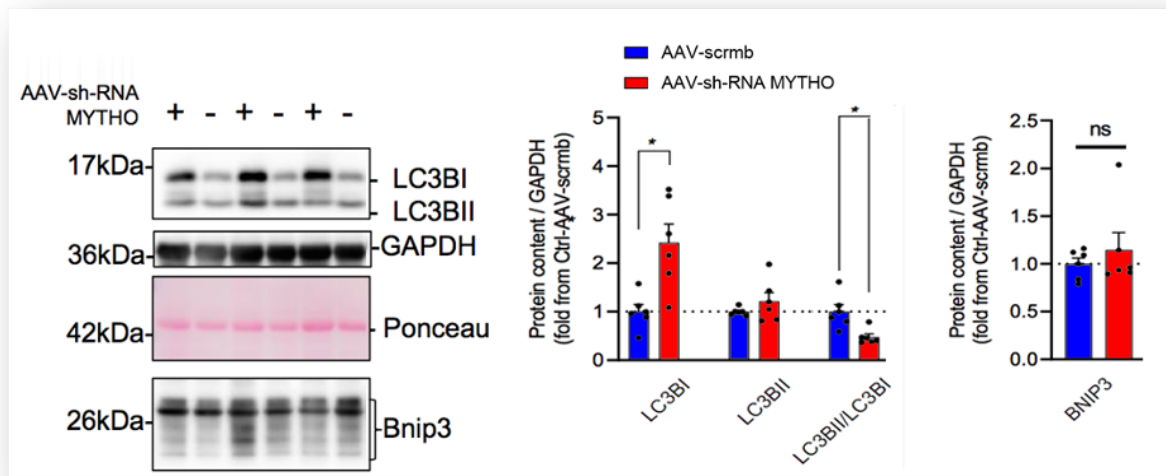


FIGURE 14

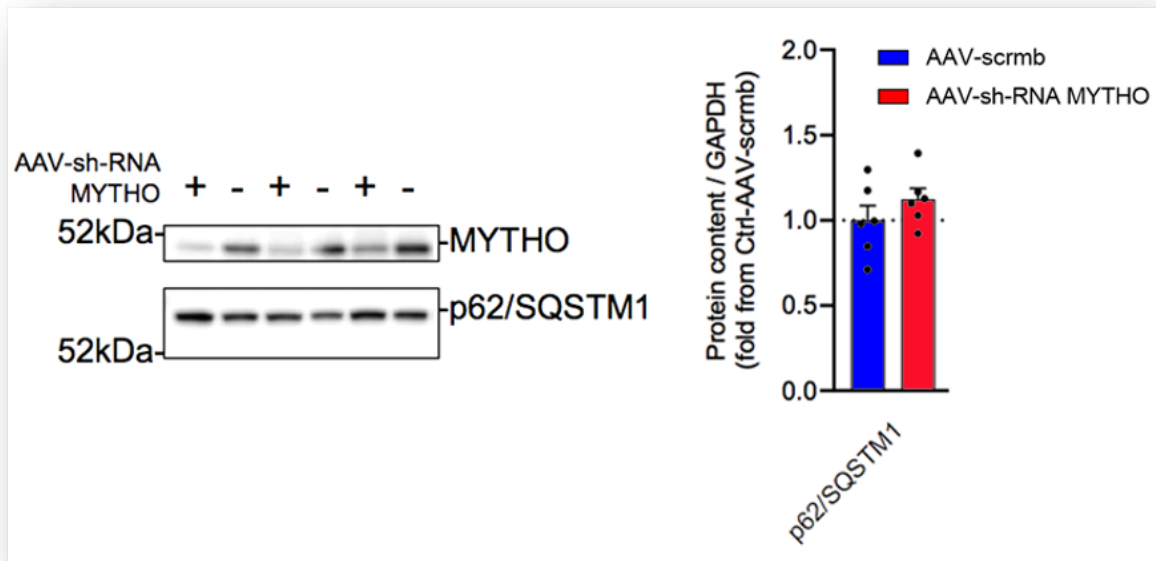


FIGURE 15

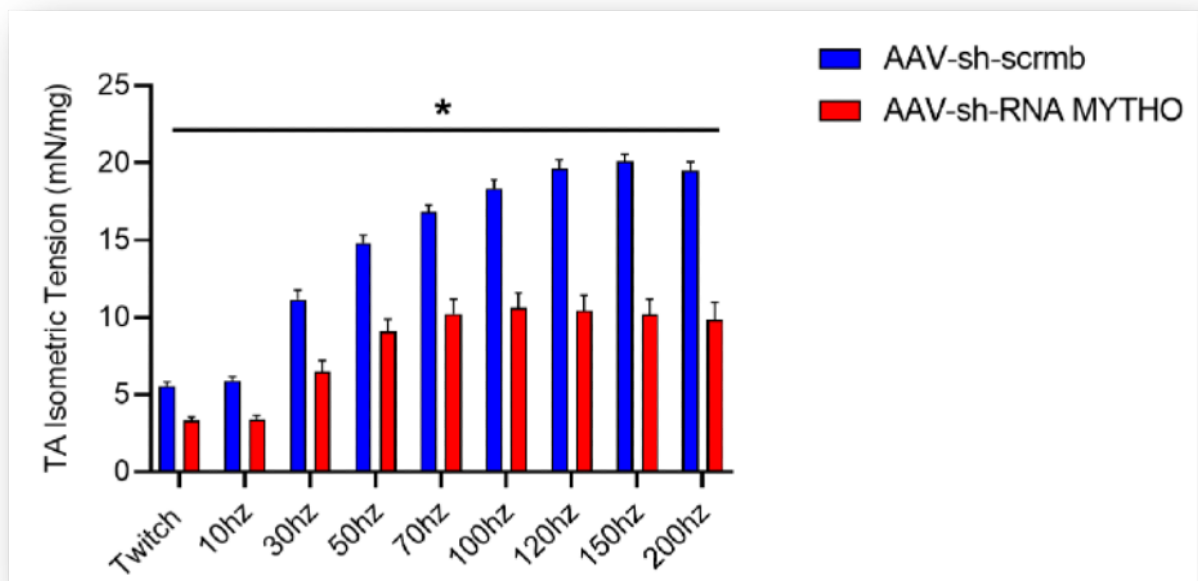


FIGURE 16

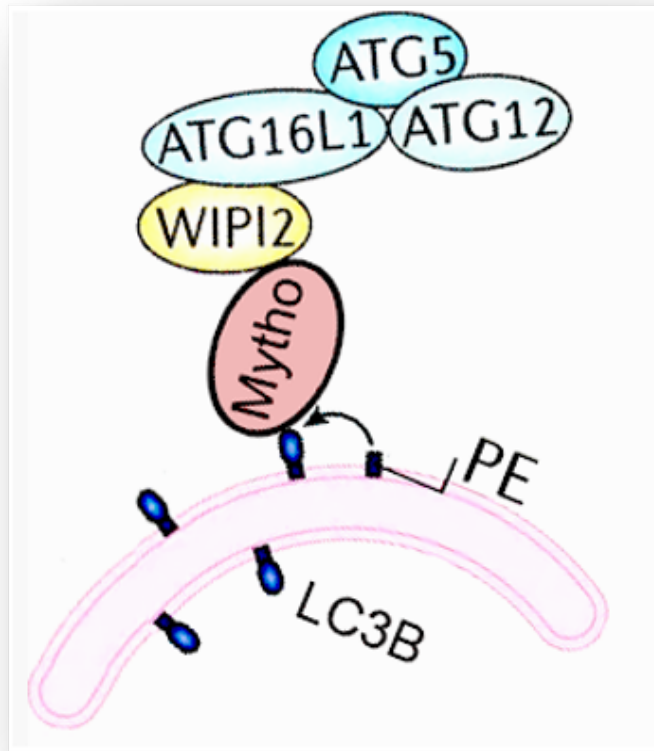


FIGURE 17

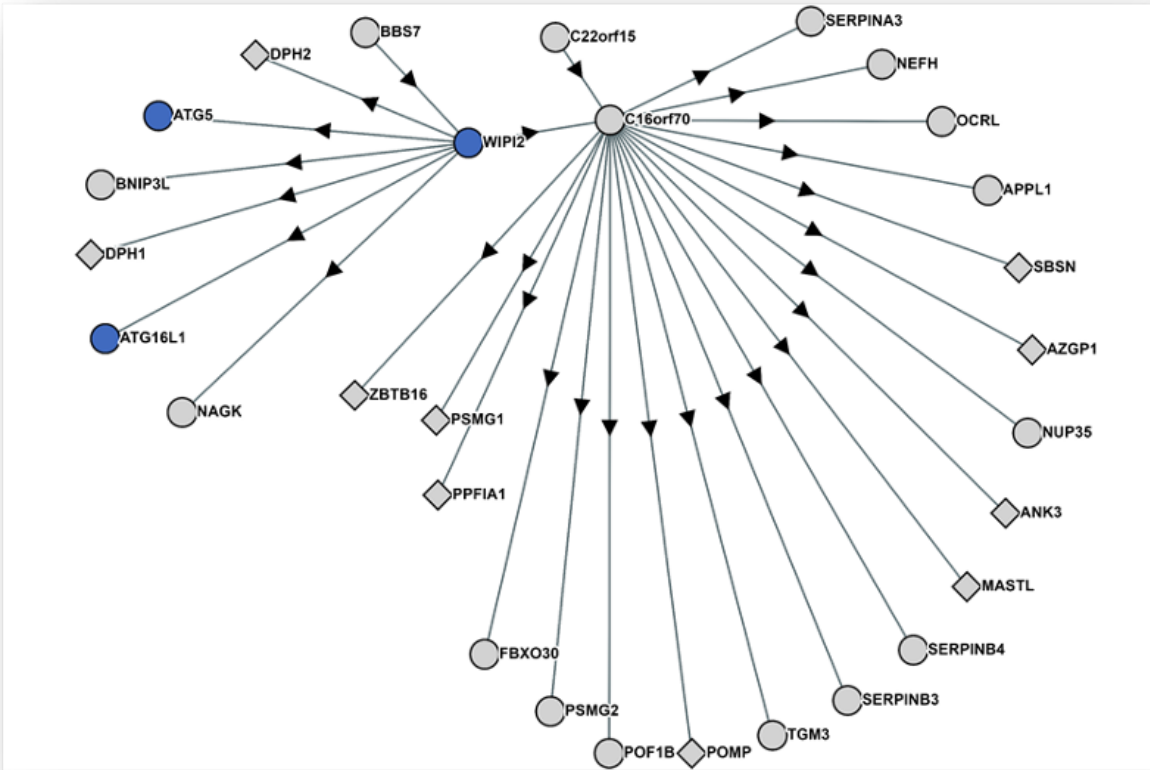


FIGURE 18

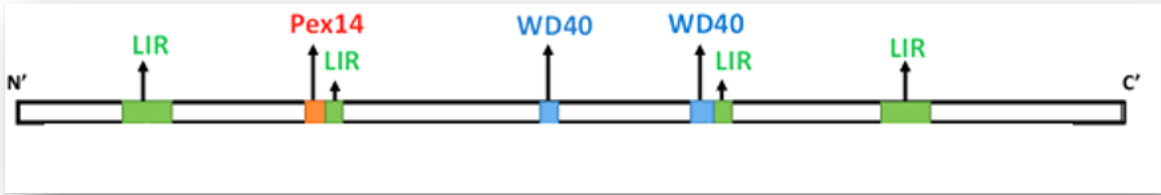


FIGURE 19

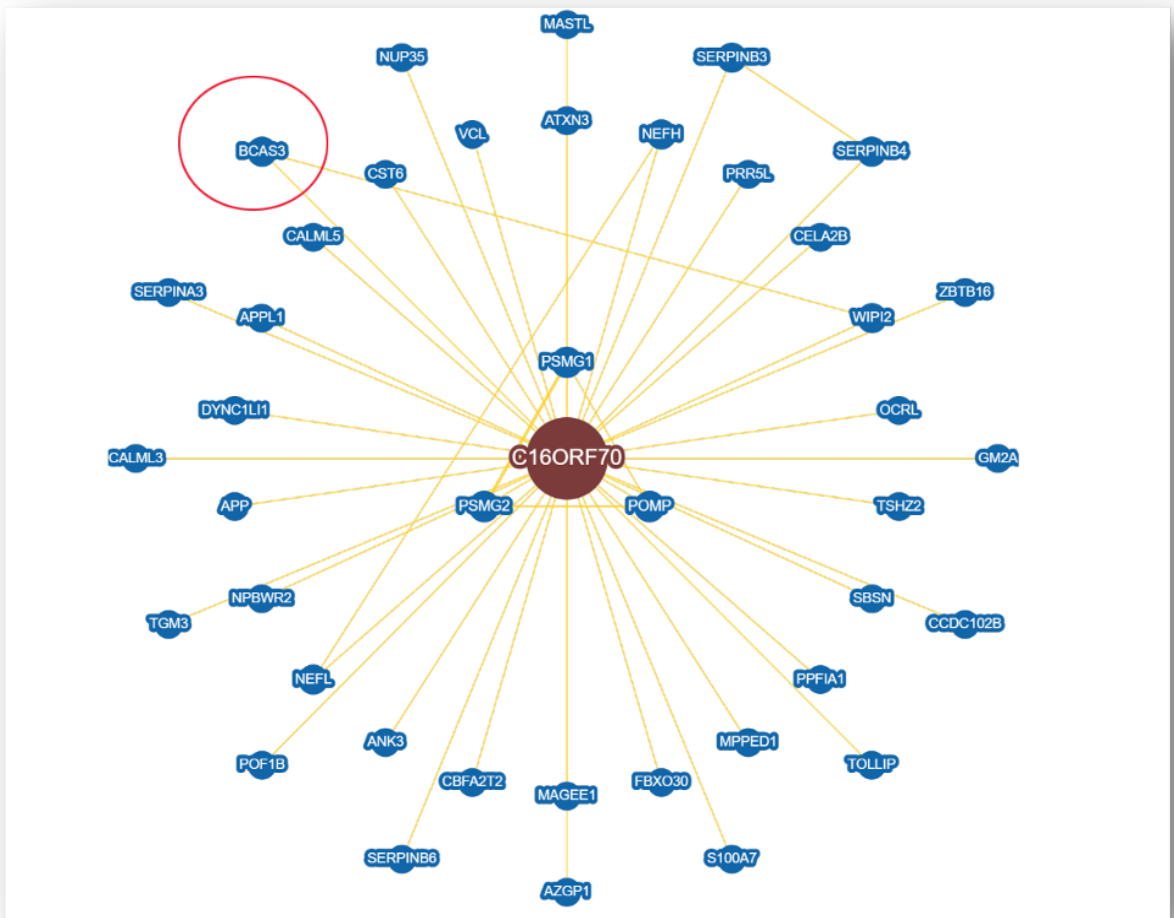


FIGURE 20

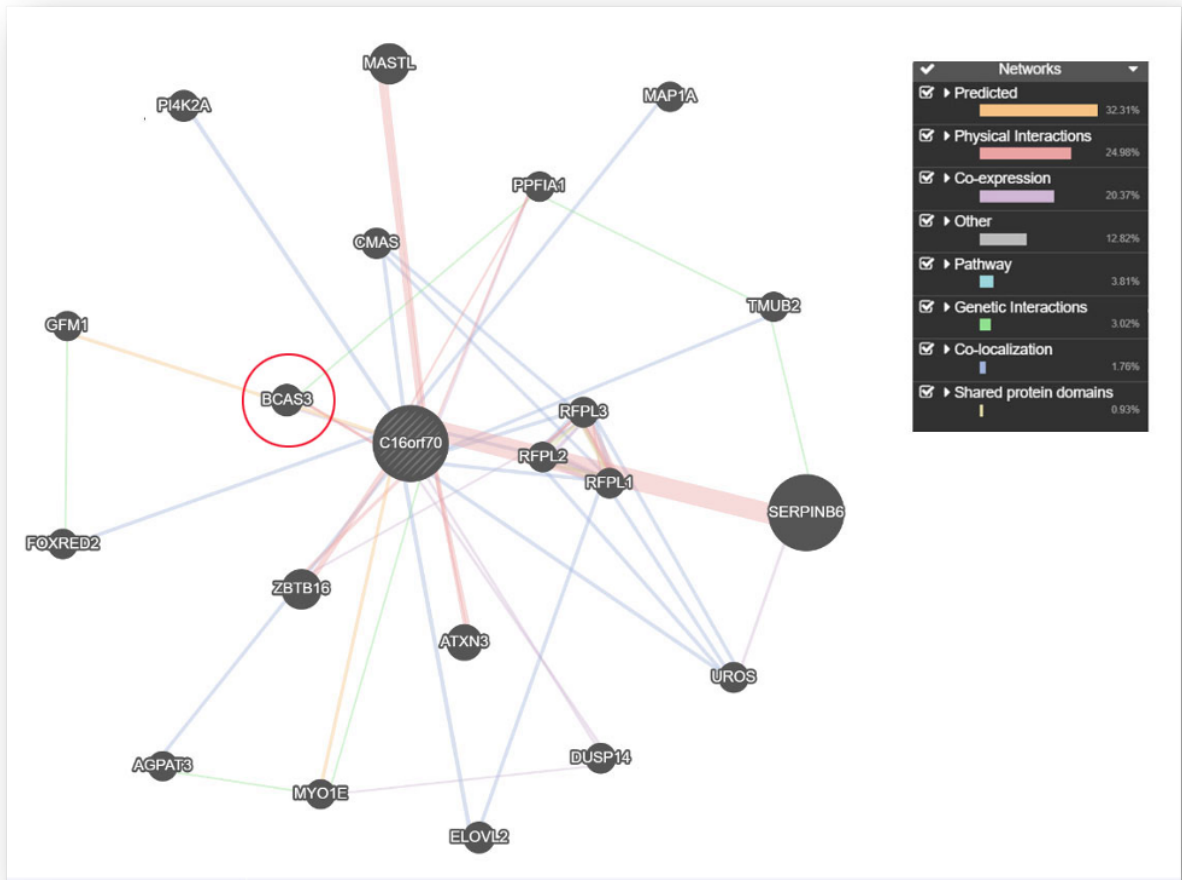


FIGURE 21



FIGURE 22

SECTION 8: FIGURE LEGENDS

Figure 1: Experimental procedures and protocols. The panel provides information on the location and timing of AAV-shRNA-ScrmB and AAV-shRNA-MYTHO i.m. injections for knocking down MYTHO (D230025D16RIK, in mouse). The AAVs were serotype 1, a serotype with a proven tropism for skeletal muscle cells (U6 refers to the promoter). Mice were euthanized 12 weeks post AAV injection and limb muscles were collected for various analyses.

Figure 2: Representative MYTHO immunoblotting in tibialis anterior (TA) muscle lysates collected 12 weeks post AAV injection. Injection of AAV-shRNA-MYTHO significantly decreased the expression of MYTHO protein relative to contralateral TA injected with AAV-shRNA-ScrmB. Ponceau staining indicate equal loading across lanes.

Figure 3: Successful MYTHO KD using i.m. AAV injections in skeletal muscles of mice. **A,** **B:** qPCR analysis of MYTHO expression levels in the tibialis anterior (TA) and the gastrocnemius (GAS) muscles injected with either AAV-shRNA-ScrmB or AAV-shRNA-MYTHO. **C:** Quantification of MYTHO protein content in TA muscles using immunoblotting. Data in bar graphs are presented as means \pm SEM. Individual animal values are shown as block dots. * $P < 0.05$, compared to AAV-shRNA-ScrmB.

Figure 4: The impact of MYTHO KD on skeletal muscle mass. **A:** Representative image demonstrating that muscles injected with AAV-shRNA-MYTHO are bigger than muscles injected with AAV-shRNA-ScrmB (scale bar = 5mm). **B, C:** Quantification of TA and GAS muscle mass. Results in bar graphs are presented as means \pm SEM. Individual animal values are shown as block dots. * $P < 0.05$, compared to AAV-shRNA-ScrmB.

Figure 5: Representative cross sections of TA muscles injected with AAV-shRNA-Scrmb (upper left) and AAV-shRNA-MYTHO (upper right and bottom left) and were stained for laminin protein (red staining) and for nuclei (DAPI, blue staining). Notice the number of small fibres with one or more central nuclei in muscles injected with AAV-shRNA-MYTHO. Bottom right: means \pm SEM of centrally nucleated fibres in the TA muscle samples. *P<0.05, compared to AAV-shRNA-Scrmb.

Figure 6: Left: Means \pm SEM of total number of muscle fibres in TAs injected with AAV-shRNA-MYTHO and AAV-shRNA-Scrmb. *P<0.05, compared to AAV-shRNA-Scrmb. Right: Means \pm SEM of median values of minimum Feret diameters of TAs injected with AAV-shRNA-MYTHO and AAV-shRNA-Scrmb. Individual muscle values are shown as black dots.

Figure 7: Means \pm SEM of minimum Feret diameters of TAs injected with AAV-shRNA-MYTHO and AAV-shRNA-Scrmb. Number of animals indicated in bars, where applicable. *P<0.05, compared to AAV-shRNA-Scrmb.

Figure 8: A: Representative images of cross sections of TAs injected with AAV-shRNA-MYTHO and AAV-shRNA-Scrmb. Scale bar 100 μ m. DAPI (blue staining) and anti-mouse IgG secondary antibody (red staining). Fibres identified with arrows were positively stained with anti-mouse IgG. **B:** Quantification of IgG-positive fibres per muscle section. *P<0.05, compared to AAV-shRNA-Scrmb.

Figure 9: A: Representative images of cross sections of TA muscles injected with AAV-shRNA-MYTHO and AAV-shRNA-Scrmb stained with three antibodies selective to type

IIA, IIB, and IIX of MyHC protein isoforms. **B**: Means \pm SEM of proportions of type IIA, IIX, IIA/IIX, and IIB in the TA muscles injected with AAV-shRNA-MYTHO and AAV-shRNA-Scrm. *P<0.05, compared to AAV-shRNA-Scrm. **C**: Means \pm SEM of minimum Feret diameters of type IIA, IIX, IIA/IIX, and IIB in the TA muscles injected with AAV-shRNA-MYTHO and AAV-shRNA-Scrm. *P<0.05, compared to AAV-shRNA-Scrm.

Figure 10: Means \pm SEM of mRNA levels of embryonic (*Myh3*) and neonatal (*Myh8*) MyHC isoforms, *MyoD* and *Myogenin* transcription factors in TA in response to injections of AAV-shRNA-Scrm and AAV-shRNA-MYTHO. *P<0.05, compared to AAV-shRNA-Scrm.

Figure 11: Representative TEM images of white GAS muscles injected with AAV-shRNA-Scrm. Top panel is showing magnified images of intermyofibrillar mitochondria, T-tubule and sarcoplasmic reticulum. Bottom panels are showing normal morphology of these structures.

Figure 12: Representative TEM images of white GAS muscles injected with AAV-shRNA-MYTHO. **A, B & D**: Accumulation of tubular aggregates and dilated sarcoplasmic reticulum. **B & F**: Abnormally shaped intermyofibrillar and subsarcolemmal mitochondria. **C**: Black arrow indicates glycogen spots. **E & F**: White arrows indicate lamellar bodies.

Figure 13: Means \pm SEM of mRNA levels of various autophagy-related genes in the TA muscles injected with AAV-shRNA-MYTHO. Values are expressed as fold from those measured in TA injected with AAV-shRNA-Scrm. *P<0.05, compared to AAV-shRNA-Scrm.

Figure 14: Representative immunoblots and means \pm SEM of LC3B, GAPDH, and BNIP3 protein levels in TA muscles injected with AAV-shRNA-Scrm and AAV-shRNA-MYTHO. *P<0.05, compared to AAV-shRNA-Scrm. NS refers to non-significant.

Figure 15: Representative immunoblots and means \pm SEM of p62/SQSTM1 protein levels in TA muscles injected with AAV-shRNA-Scrm and AAV-shRNA-MYTHO. Also shown is MYTHO protein blot, to indicate the degree of KD.

Figure 16: Means \pm SEM of *in-situ* isometric tension generated by TA muscles in response to various stimulation frequencies. It should be noted that TA contractility was measured in one hindlimb for a given animal. *P<0.05, compared to AAV-shRNA-Scrm.

Figure 17: Proposed mechanism through which MYTHO regulates the elongation step of autophagosome formation.

Figure 18: Predicted MYTHO (C16orf70) interactome as revealed by *BioPlex* webtool. Highlighted in blue color are proteins involved in autophagosome formation.

Figure 19: Structure of MYTHO protein showing WD40 domains and LIR motifs.

Figure 20: MYTHO (C16orf70) protein interactome based on *BioGRID* webtool. Note that MYTHO physically interacts with BCAS3 protein.

Figure 21: MYTHO (C16orf70) protein interactome based on *GeneMANIA* webtool. Note that MYTHO protein physically interacts with BCAS3 protein.

Figure 22: Lamellar bodies (black arrows) detected in white GAS muscle with MYTHO knockdown. Note the onion shaped structures localized in the intermyofibrillar space in this example. Also note that the lamellar body on the left is fully formed while the one on the right is in the process of being fully developed.